

# Pursuing mechanisms of extracellular vesicle formation. Effects of sample processing

Darja Božič<sup>a,b,\*</sup>, Matej Hočvar<sup>c</sup>, Veno Kononenko<sup>d</sup>, Marko Jeran<sup>a,b</sup>,  
Urška Štibler<sup>b</sup>, Immacolata Fiume<sup>e</sup>, Manca Pajnič<sup>a</sup>, Ljubiša Pađen<sup>a</sup>,  
Ksenija Kogej<sup>f</sup>, Damjana Drobne<sup>d</sup>, Aleš Iglič<sup>b,e,g</sup>,  
Gabriella Pocsfalvi<sup>e</sup> and Veronika Kralj-Iglič<sup>a,e</sup>

<sup>a</sup>Laboratory of Clinical Biophysics, Faculty of Health Sciences, University of Ljubljana, Ljubljana, Slovenia

<sup>b</sup>Laboratory of Physics, Faculty of Electrical Engineering, University of Ljubljana, Ljubljana, Slovenia

<sup>c</sup>Department of Physics and Chemistry of Materials, Institute of Metals and Technology, Ljubljana, Slovenia

<sup>d</sup>Department of Biology, Biotechnical Faculty, University of Ljubljana, Ljubljana, Slovenia

<sup>e</sup>Extracellular Vesicles and Mass Spectrometry Laboratory, Institute of Biosciences and BioResources (IBBR), National Research Council of Italy (CNR), Naples, Italy

<sup>f</sup>Department of Chemistry and Biochemistry, Faculty of Chemistry and Chemical Technology, University of Ljubljana, Ljubljana, Slovenia

<sup>g</sup>Laboratory of Clinical Biophysics, Faculty of Medicine, University of Ljubljana, Ljubljana, Slovenia

\*Corresponding author: E-mail: Darja.Bozic@fe.uni-lj.si.

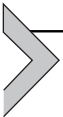
## Contents

1. Introduction	114
2. Experimental	117
2.1 Sample collection	117
2.1.1 Blood collection and plasma preparation	117
2.1.2 EV isolation from fresh plasma	118
2.1.3 EV isolation from thawed plasma	119
2.2 Scanning electron microscopy	120
2.3 Flow cytometry	121
2.4 Dynamic light scattering	121
2.5 Proteomic analysis	122
3. Results	122
3.1 Low speed isolation protocol analysis	122
3.2 Parallel centrifugation experiment	127
3.2.1 Analysis of the changes in protein profiles	132
4. Discussion	134
4.1 Source of vesicles in the isolates	134
4.2 Isolation efficiency	140
4.3 Identity of particles in EV isolates (EVs' genuineness)	141
5. Conclusions	143
6. Appendix	143

6.1 Flow cytometry	143
Acknowledgments	151
References	151

## Abstract

Although the role of extracellular vesicles in inter-cell communication is acknowledged, their analytics is yet problematic. Poor understanding of effects of sample processing may be one of the cornerstones of this issue. We investigated the effects of centrifugation during the vesicle isolation on the number, size, content and shape of particles in the isolates. Particles in the range of about 100–500 nm as observed by the scanning electron microscope exhibited characteristic shapes of vesicles without internal structure. Enhanced centrifugal pull resulted in increased amount of certain types of proteins in the isolates. Majority of present proteins were highly abundant human plasma proteins, including albumins and immunoglobulins. Results are in favor of the hypothesis that the isolated particles reflect the substance from which they originate (cells and the surrounding solution) and the performed processing; and therefore, vesicles in isolates should be viewed upon as a dynamic material with transient identity.



---

## 1. Introduction

Nano- to micro-sized membrane enclosed particles (vesicles) can be found in biological fluids and cell-culture media. Initially, they were called “cell dust” [1] as they were presumed to be packages of cell waste and/or a side product of cell degradation. It was later observed that they intervene in various biological processes and play important roles in development and functioning of an organism [2]. Different mechanisms of their formation were proposed, and a term extracellular vesicles (EV) was introduced to comprise the heterogeneous cluster of vesicles that can be found in biological samples.

EVs have cell-originated membrane and contain important biological molecules (proteins, lipids, nucleic acids and metabolites). Therefore, EVs are carriers of valuable information about the cells they come from, reflecting their state and condition. The foreseen potential of EVs to be used as a convenient diagnostic and potentially therapeutic tool opened an era of extensive research. However, up to day, EV analytics has not reached the level of reliability required for clinical applications. Thus, EV exploitation remains limited [3–8].

One of the bottlenecks of the progress appears to be EV harvesting, their isolation and purification [9–13]. Despite strong initiatives for

standardization of these procedures [14–16], the studies of EVs remain largely incoherent. The reproducibility of the isolation experiments and also the reliability of the following characterization and functional data is deficient. The need of improvement of the existing protocols pushes the researchers into further and further changes of parameters and development of completely new approaches. Due to the high variety of methodologies, the outcomes of different studies are often hard to compare. But since the reliable and reproducible method for EV isolation is still lacking, and we do not have enough knowledge of how individual parameters influence the isolation, the standardization of protocols seems to be yet premature.

Events taking place during harvesting are still poorly understood, and processing of samples before and during the isolation procedure can cause significant changes of the EVs in the isolates [17]. Genuineness of EVs after isolation and purification procedures may be questionable and represent a big problem in the EV field. Have we crossed from disregard of the “cell dust” to some level of over-/miss-price of the microparticles’ significance in the severely processed samples? We think, that in order to improve EVs’ applicability, their stability must be more closely considered, primarily regarding rigidity/fluidity of the membranes and their remodeling.

The self-assembly of a biological membrane is based on the equilibrium of its components, which is on one hand directed by the cell itself (through production and regulation of membrane components) and on the other, influenced by the external factors such as chemicals, temperature, and pressure. When the constraints shaping the membrane assembly are changed, its components face a possibility (/necessity) to rearrange according to new conditions of the system. By the physical laws, the new arrangement represents the most easily accessible free energy minimum.

The membrane architecture varies from cell to cell in regard to its functionality and physiological state. The flexibility of a membrane-perimembrane construct conditions its sensitivity and response to perturbations. Disruptions may be followed by membrane spontaneous reformulation (resealing, vesicle formation) or degradation (collapse or dissociation of components).

The most common method for EV isolation from liquid samples is differential centrifugation (DC) [10,18]. Centrifuge tubes containing samples are placed in a centrifuge, where spinning creates a centrifugal field in the system that pulls the freely floating particles in the samples away from the centrifuge rotor axis. Separation is based on distinctive sedimentation coefficients ( $S$ ) of the sample components. Sedimentation coefficients depend on

particles' mass ( $m$ ), radius ( $r$ ) and on viscosity of the medium ( $\eta$ ), according to relation  $S = m/6\pi r\eta$ . Differential centrifugation (DC) is therefore a centrifugation method in which different species are selectively spun down from a mixture by a series of increasing centrifugal forces. General pitfalls of DC include variability in sedimentation efficiencies [19,20], accompanied with co-sedimentation of undesired material (proteins and lipoproteins [21–23], RNA aggregates [24], viral particles) with similar  $S$  value; and EV aggregation and/or disruption [12,25,26]. However, in spite of vast use of ultracentrifugation-based processes, the knowledge on the effect of high centrifugal force and the concentrating of EVs throughout the sample processing is yet rudimentary.

Due to their small size, a prolonged action (hours) of a strong force (high speed centrifugation, ultracentrifugation, UC) is required to sediment EVs. The time consumption of the procedure paralyzes the high-strength studies with large number of samples, and makes EV centrifugation inconvenient for routine use in clinical practice. Alternative isolation techniques were recently proposed to overcome these issues. Ultrafiltration, flow field-flow fractionation, dialysis, size exclusion chromatography, microchip-based techniques and precipitation-based methods are being developed, and used alone or in combination with ultracentrifugation-based methods. Immunoaffinity-based isolation can also be applied to harvest EVs with particular surface protein composition [27–29]. Recently, commercial kits were launched, e.g. ExoQuick (System Biosciences) and Total Exosome Isolation kits (TEI, Invitrogen) based on polymer precipitation, qEV (Izon) based on size exclusion chromatography, (UF, Millipore) based on ultrafiltration, and exoEasy (Qiagen) based on membrane-based affinity binding [30]. However, different isolation methods were found to lead to different EV populations and different level of purity of the EV isolates [31]. Furthermore, damage or alteration to the EV structure may occur during the harvesting and assessment procedures, due to mechanical/thermal stress and chemical reactions. Although the suggested methods are faster and easier to apply than DC, a recent thorough comparison between isolates that were obtained by various methods showed that among the tested, ultracentrifugation-based methods are still preferential as regards the isolate purity [30]. Also, with available centrifuge and high throughput of samples, this technique may prove cost-effective and environment-labile.

To improve the repeatability and accuracy of the isolation procedure we examined the effects of centrifugation on biological material. In order to reveal what happens with the plasma components that are not successfully

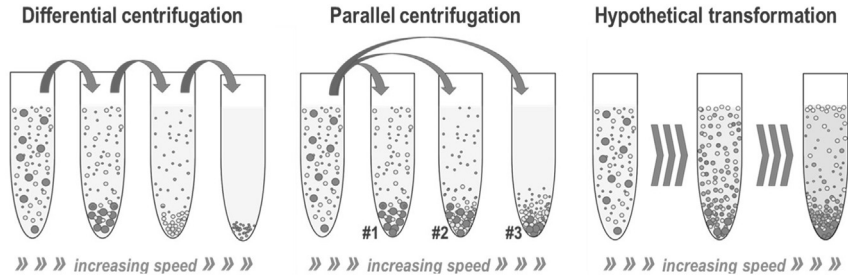
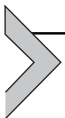


**Fig. 1** Schematic representation of centrifugation approaches. Differential centrifugation is a common method for separation of particles with different sedimentation coefficients. Larger and denser particles have higher sedimentation rate, and therefore concentrate in the pellet faster than smaller and thinner ones. Low speed centrifugation is therefore used to remove cells and larger particles, while supernatant is subjected to higher speed centrifugation to sediment smaller particles. The parallel centrifugation was performed in this study to test the hypothesis of sample transformation during harvesting, and investigate possibilities of tearing of particles and reorganization of the present components upon centrifugation processing.

removed in the appropriate steps of DC, blood plasma was subjected to parallel centrifugation (schematic comparison of centrifugation-based approaches is represented in Fig. 1). Different centrifugation accelerations were tested, starting from lower (i.e. 10 000 g), and ending with 100 000 g, which is commonly used to harvest small EVs (exosomes) [10]. A protocol that is frequently used for clinical studies [17,32–46] was also inspected. We closely followed the transformation of the material from mild to the keenest conditions. Flow cytometry (FCM) and dynamic light scattering (DLS) were employed for particle quantification and size characterization. Attention was paid to the effects of freezing/thawing of the starting sample, and UC-processing temperature on the resulting isolates. Gel-based proteomics was performed on a set of isolates to reveal their protein content and composition. Morphology of isolates was examined by scanning electron microscopy (SEM).



## 2. Experimental

### 2.1 Sample collection

#### 2.1.1 Blood collection and plasma preparation

Blood was donated by an author of this article, a 28 years old male with no record of disease. After a 12 h overnight fast, venous blood was collected at ambient temperature (24 °C) by a 21-gauge needle (length 70 mm, inner

radius 0.4 mm, Microlance, Becton Dickinson, New Jersey). It was drawn into two 4.5 mL evacuated tubes (BD Vacutainers, Becton Dickinson, CA) with trisodium citrate (109 mM). The tubes were gently turned around three times and then centrifuged for 30 min, 2000 g (centrifuge Centric 400/R, Tehnica, Železniki, Slovenia) at 22 °C in order to separate plasma from cells. The plasma supernatant was collected (down to 4–5 mm level above the cell pellet) and pooled in a 15 mL falcon tube prefilled with 5 mL of citrate-PBS buffer (154 mM NaCl, 1.4 mM phosphate, 10.9 mM trisodium citrate; pH 7.4) at ambient temperature. Isolation of EVs from this sample was performed straight after.

Due to the large required sample volume for parallel centrifugation experiments, additional blood plasma was purchased from the Blood Transfusion Center of Slovenia. The blood sample was collected according to general standards and procedures for transfusion purposes. A complete dose of blood was collected from a healthy volunteer without complications. COMPOFLOW® 4F T&B 63 mL CPD/100 SAGM-RCC-PDS-V collecting bag (Fresenius Kabi AG, Czech Republic) was used together with scale and mixer device Hemoflow 06393. The blood was centrifuged after 3 h 20 min of incubation at room temperature, centrifugation for 14 min at 22 °C at 3540 rpm (Cryofuge 6000i, rotor 6606, Thermo Scientific, ZDA) was performed (hard spin) to separate whole blood into three components: hematocrit, plasma and the buffy coat layer. The cell fractions and blood plasma were collected by CompoMat G5 and CompoMaster Net G5 System (program of separation: TB Buffy Coat). The plasma (260 mL) was not suitable for further medical utilization due to the imperfect cell elimination. The plasma was kept at room temperature (22 °C) for 20 h before dispensed into the 15 mL aliquots, frozen and stored at –80 °C.

### **2.1.2 EV isolation from fresh plasma**

1 mL aliquots of diluted plasma were centrifuged at 17 570 g for 20 min at 22 °C (centrifuge Centric 200/R, Domel, Železniki, Slovenia, swinging rotor). 950 µL of the supernatant was saved for later analysis; pellet was washed by adding 450 µL of fresh citrate-PBS buffer and centrifuged again using the same conditions. Two EV isolate samples were fixed *in situ* (adding 50 µL of modified Karnowski's fixative to a 50 µL of sample in the tube); while the rest were resuspended in the remaining 50 µL of supernatant, and gathered (to yield app. 400 µL). Fresh buffer was added to this isolate to a total volume of 1 mL, rigorously mixed and centrifuged again using the same conditions. 700 µL of supernatant was discarded, while the pellet was suspended in the remaining liquid.

### 2.1.3 EV isolation from thawed plasma

To ensure the same starting plasma sample for evaluating effects of enhanced centrifugation through the experiments of parallel centrifugation (Fig. 1, Table 1: protocols #1a-b, #2-#10), plasma sample was purchased from Blood Transfusion Center of Slovenia and kept frozen at  $-80^{\circ}\text{C}$  until used. The frozen plasma was rapidly thawed at  $37^{\circ}\text{C}$  and centrifuged at 1 000 g, 30 min,  $22^{\circ}\text{C}$ , (centrifuge Centric 400/R, Domel, Železniki, Slovenia), to remove the remaining cells. Supernatant was transferred into another centrifuge tube and centrifuged again at 1 000 g, 15 min,  $22^{\circ}\text{C}$ . The supernatant after second step of cell removal was then dispensed into 1 mL aliquots for isolation according to different protocols.

**Table 1** List of EV isolation protocols and analyses performed on respective isolates.

Starting blood plasma sample	RCF <sup>c</sup>	Duration	<i>T</i>	Rotor type	Protocol	Analysis
Fresh <sup>a</sup>	17 500 g	20 min	$22^{\circ}\text{C}$	Swinging bucket	#1	FCM, SEM
Thawed <sup>b</sup>	17 500 g	5 min	$22^{\circ}\text{C}$	Swinging bucket	#1a	DLS, FCM, MS
Thawed <sup>b</sup>	17 500 g	30 min	$22^{\circ}\text{C}$	Swinging bucket	#1b	FCM, DLS
Thawed <sup>b</sup>	10 000 g	60 min	$22^{\circ}\text{C}$	Fixed angle	#2	FCM, MS, SEM
Thawed <sup>b</sup>	20 000 g	60 min	$22^{\circ}\text{C}$	Fixed angle	#3	FCM, MS, SEM
Thawed <sup>b</sup>	100 000 g	60 min	$22^{\circ}\text{C}$	Fixed angle	#4	FCM, MS, SEM
Thawed <sup>b</sup>	100 000 g	8 h	$22^{\circ}\text{C}$	Fixed angle	#5	FCM, MS, SEM
Thawed <sup>b</sup>	10 000 g	60 min	$8^{\circ}\text{C}$	Fixed angle	#6	DLS, FCM
Thawed <sup>b</sup>	20 000 g	60 min	$8^{\circ}\text{C}$	Fixed angle	#7	DLS, FCM
Thawed <sup>b</sup>	50 000 g	60 min	$8^{\circ}\text{C}$	Fixed angle	#8	DLS, FCM
Thawed <sup>b</sup>	100 000 g	60 min	$8^{\circ}\text{C}$	Fixed angle	#9	DLS, FCM
Thawed <sup>b</sup>	100 000 g	120 min	$8^{\circ}\text{C}$	Fixed angle	#10	DLS, FCM

DLS, dynamic light scattering; FCM, flow cytometry; MS, mass spectrometry. SEM, scanning electron microscopy.

<sup>a</sup>The blood plasma was prepared from fresh blood sample. Note that the donor and the plasma preparation procedure were different for this protocol than for all the rest.

<sup>b</sup>In order to assure the same starting sample for all tested protocols, blood plasma was purchased from Blood Transfusion Center of Slovenia. Due to the limitations of throughput of the method, the experiments were not performed on the same day. The plasma was therefore frozen and stored at  $-80^{\circ}\text{C}$  until used.

<sup>c</sup>Relative centrifugal forces (RCF) of the isolation and purification step of the protocol.

Isolation was performed in centrifuge Centric 200/R (Domel, Železniki, Slovenia, with swinging rotor); at 17 570 g for 5 min (protocol #1a) or 30 min (protocol #1b) at 22 °C; or in the Beckman L8-70 M ultracentrifuge (Beckman coulter, USA, with fixed angle rotor type Ti50.2) at 10 000 g (protocol #2) or 20 000 g (protocol #3) or 100 000 g (protocol #4) at 22 °C for 1 h or at 100 000 g and 22 °C for 8 h (protocol #5). 950 µL of supernatant was discarded; the pellet was resuspended in 1 mL of citrate-PBS buffer and centrifuged again. In the sample obtained by high velocity centrifugation (8 h, 100 000 g pellet), the whitish fraction just above the gelatinous pellet was resuspended in 1 mL of buffer and centrifuged again at 100 000 g for 4 h. The supernatant was discarded and the fraction above the gelatinous part (cca 50 µL) was resuspended in 450 µL of fresh buffer. The experiment was repeated at 8 °C, applying 10 000 g (protocol #6), 20 000 g (protocol #7), 50 000 g (protocol #8) and 100 000 g (protocol #9) for 1 h, and 100 000 g for 2 h (protocol #10).

## 2.2 Scanning electron microscopy

The samples were fixed in a modified Karnovsky's fixative (2.5% glutaraldehyde, 0.4% formaldehyde in phosphate buffer saline (PBS; 137 mM NaCl, 2.68 mM KCl, 10.14 mM Na<sub>2</sub>HPO<sub>4</sub>, and 1.84 mM KH<sub>2</sub>PO<sub>4</sub>, pH 7.4) and post-fixed with OsO<sub>4</sub>, following the protocol adopted from Lešer et al. [47]. In brief, the supernatant after the centrifugation at 17 570 g was applied to a 0.05-µm filter (Polycarbonate (PCTE) membrane filters, ref: PCT00513100, Sterlitech, USA), lightly washed with PBS and fixed in the primary fixative for 1 h at 22 °C. The pellets were fixed in the tubes directly, or transferred to a clean cover glass and incubated for 2 h at room temperature to allow adhesion. Primary fixative (buffered glutaraldehyde and paraformaldehyde) was then added to all the samples in the ratio 1:1, and the samples were incubated overnight at 4 °C. The fixatives were then removed by three-step washing (incubation time 10 min in each step) with phosphate buffer. Then, samples were incubated in 2% OsO<sub>4</sub> for 1 h, washed 3-times with distilled water (incubation time 10 min in each step), treated with saturated water solution of thiocarbohydrazide (15 min), washed with distilled water (incubation time 10 min in each step), incubated 1 h in 2% OsO<sub>4</sub>, again; washed three-times with distilled water (incubated for 10 min in each step) and dehydrated in graded series of ethanol (30%–100%, 10 min each; absolute ethanol was replaced 3 times) and hexamethyldisilazane (mixed with absolute ethanol; 30%, 50% and

100%, 10 min each), and finally air dried. The samples were Au/Pd coated (PECS Gatan 682), and examined using a JSM-6500F Field Emission Scanning Electron Microscope (JEOL Ltd., Tokyo, Japan).

### 2.3 Flow cytometry

FCM measurements were performed with MACS QUANT flow cytometer (Miltenyi, Bergisch-Gladbach, Germany), with the lasers set to 394 V (FSC), 454 V (SSC), and the trigger set to SSC: 1.8). Blood and platelet poor plasma were analyzed within 2 h from blood collection. The particles in fresh isolates were analyzed by flow cytometry immediately after isolation, and later, on thawed samples after up to a week of storage at 4 °C. The gates were set in a preliminary study of several blood samples; identity of cells in the presented regions was confirmed by fluorescently labeled antibodies (CD41 was used to label platelets and CD45 to label leukocytes) and by SEM analysis.

### 2.4 Dynamic light scattering

The dynamic light scattering experiments were performed with the 3D-DLS-SLS cross-correlation spectrometer from LS Instruments GmbH (Fribourg, Switzerland) with a 20 mV He–Ne laser (Uniphase JDL 1145P,  $\lambda_0 = 632.8$  nm). The samples were equilibrated in the decalin bath at 25 °C for 15 min prior the measurement. The measurements were performed at 90° angle. All details regarding the instrumentation and data treatment are described in detail in Refs. [48–50]. The samples were diluted with the citrate-PBS in the ratio 1:10 or 1:20 to attain optimal scattering intensity and eliminate impacts of high concentration on particle diffusion. CONTIN analysis [51] was employed for transformation of correlation functions into the distribution of diffusion coefficient ( $D$ ) values of species in solution. The final result of the analysis is the size distribution of particles in solution. The size parameter obtained is the hydrodynamic radius ( $R_h$ ), which is calculated from the measured  $D$  by taking into account the Stokes–Einstein relation ( $D = k_B T / 6\pi\eta R_h$ ; here,  $k_B$  is the Boltzmann constant,  $T$  is the temperature and  $\eta$  is the viscosity of the medium). As samples were very dilute, water viscosity was considered appropriate for calculation of  $R_h$  from the measured diffusion coefficient. The  $R_h$  calculated in this way corresponds to the radius of a hypothetical hard sphere that has the same  $D$  as the particles in the sample. A representative distribution as obtained by the DLS analysis is presented in Fig. 2 for an isolate and its corresponding plasma supernatant after the first step of isolation.

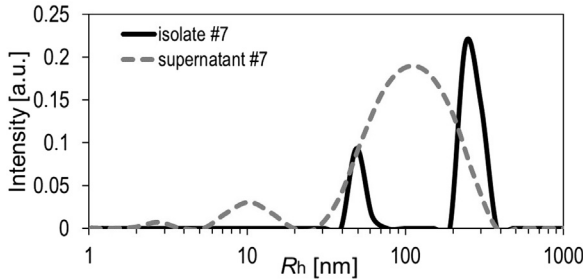
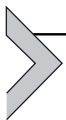


**Fig. 2** A representative size distribution as obtained by the DLS analysis of an isolate and the corresponding plasma supernatant after first step of isolation. Intensity of scattering ( $I$ ) given in arbitrary units (a.u.) represents the fraction of intensities  $I_{Rh}/I_{tot}$ .

## 2.5 Proteomic analysis

The protein contents of different isolates (obtained by centrifugation at 22 °C; assigned as isolate 1–5) were determined by Bicinchoninic acid (BCA) protein assay kit (Pierce, Thermo Scientific, USA). Volumes containing 20  $\mu$ g of protein were loaded and electrophoretically separated under reducing conditions on a precast Novex Bolt 4%–12% Bis-Tris Plus gel using Bolt (3-(N-morpholino)propanesulfonic acid) MOPS SDS running buffer (Life Technologies, Carlsbad, CA, USA) according to the manufacturer's instructions, and stained with colloidal Coomassie blue. Seven bands were selected for LC-MS/MS based shotgun proteomics analysis. Details regarding MS and bioinformatics are described in Refs. [52–54].



## 3. Results

### 3.1 Low speed isolation protocol analysis

An isolate was prepared from fresh plasma sample according to the protocol #1 (Table 1) that was found to be frequently employed in clinical studies. As this protocol applies relatively low centrifugation forces (17 570 g), larger particles were expected to be present in the isolate, while the smaller ones shall be removed in the washing step.

Fig. 3 shows SEM images of the surface of the centrifuge tube in which the last step of the isolation of EVs from the fresh blood sample by the protocol #1 had been performed. Activated platelets accumulated in the bottom of the centrifuge tube (Fig. 3A), while many damaged ones were found in the region of transition from the bottom to the wall (Fig. 3B). There were many submicron particles of various shapes attached to the

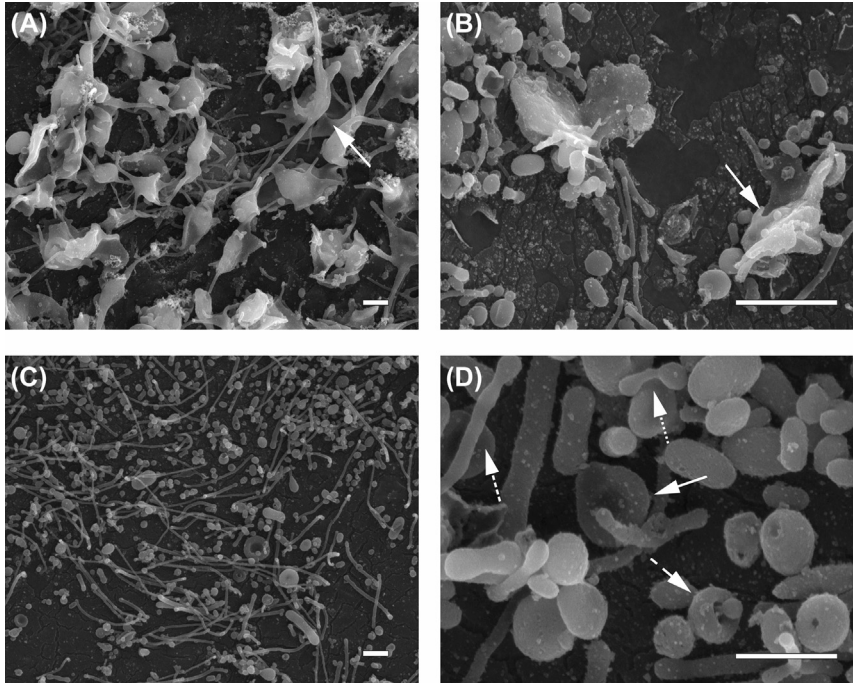


**Fig. 3** Scanning electron microscopy images of isolates from human blood plasma obtained by protocol #1 (17 570 g, 22 °C, 20 min, [Table 1](#)) and imaged directly in the microcentrifuge tube in which the last step of the isolation took place. (A) The platelets that were not successfully removed in the first step of isolation gather in the pellet after centrifugation at 17 570 g. The activated platelets exhibit tubular protrusions (an example exposed by the *white arrow*). (B) Damaged platelets surrounded by vesicles; the white arrow points to a corpus of a platelet with stumps that probably remained after projections were torn away during processing, (C) diversely shaped structures were found adhered to the centrifuge-tube wall. (D) High magnification micrograph of those structures. Arrows point to some characteristic shapes corresponding to the theoretical free-energy minimum conformations of membrane bilayer [17,55]: biconcave discoid (*full line arrow*), globular units joined by neck-straits (*dotted arrow*), tubes (*short-dashed arrow*), torus (*long-dashed arrow*). Scale bars in (A–C): 1  $\mu\text{m}$ ; and 500 nm in (D), respectively.

surface higher up in the centrifuge-tube ([Fig. 3C–D](#)). The smooth spherical endings of the observed tubular structures ([Fig. 3D](#), short dashed arrow) suggest that these particles have membranous foundation. The pattern of their orientation ordering (see [Fig. 3C](#)) is probably caused by the flow of the sample established upon centrifugation.

[Fig. 4](#) shows SEM images of the same EV isolate as presented in [Fig. 3](#), but in this case, the same isolate was transferred and fixed for SEM imaging

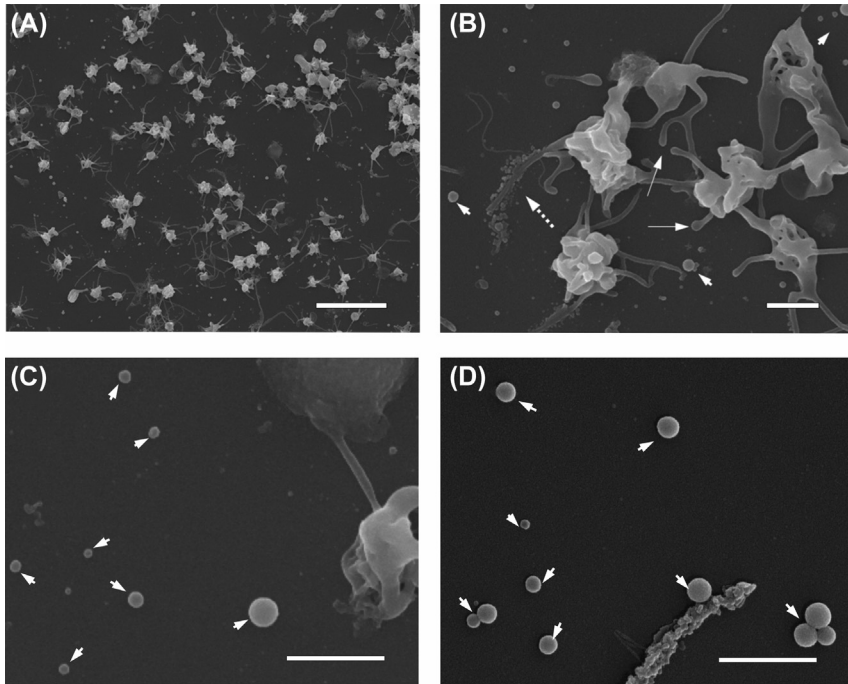


**Fig. 4** Scanning electron microscopy images of isolates from human blood plasma obtained by protocol #1 (17 570 g, 22 °C, 20 min, [Table 1](#)) imaged after transferring the isolate to a cover glass. (A) residual platelets adhered to the glass surface, (B) and (C) close-ups of selected regions; (D) a coverglass (with no biological material) treated by the same fixation protocol as samples of isolates. The full-line arrows point to thickened endings of tubular protrusions. The dotted arrow shows a group of small (nano-sized) particles. Arrowheads point to artifacts of fixation (a close up on (C) that were also found in blank samples (D)). Scale bars: 10  $\mu\text{m}$  in (A), and 1  $\mu\text{m}$  in (B–D).

on a cover-glass. The activated platelets from the isolate adhered to the cover-glass ([Fig. 4A](#)). Some small structures (10–50 nm) of very regular round shape (arrowheads on the close-ups in [Fig. 4B](#) and [C](#)) were noted in the isolates. Similar structures were observed also in samples where no biological material was present ([Fig. 4D](#)), and were therefore considered artifacts of sample preparation. Only few particles with characteristic shapes of vesicles (such as the ones in [Fig. 3B–D](#)), were observed in this sample.

[Fig. 5](#) shows the supernatant of the plasma after the first centrifugation (the part of the sample which was discarded in the process of isolation). The supernatant was transferred to the filter paper for imaging. Neither intact nor activated platelets were observed in the supernatant. Fragments of membranes (arrowheads) and some globular particles (full-line arrows)

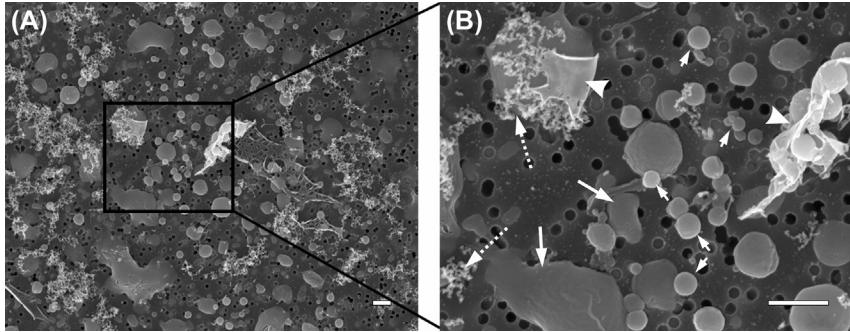


**Fig. 5** Scanning electron microscopy images of the supernatant of plasma centrifuged by protocol #1 (17 570 g, 22 °C, 20 min, [Table 1](#)) – (A) and a close up of it – (B) Fragments of membranes (thick arrowheads), loose globular particles splotted on the surface of the filter (*full-line arrows*), meshwork precipitates (*dotted arrows*) and probable artifacts of fixation (*small arrows*). Scale bars: 1  $\mu\text{m}$ .

were noted, many of which were splotted on the surface of the filter. Some meshwork precipitates were also observed in this sample (dotted arrows). They could have been formed during fixation by aggregation of organic components. Such structures were often observed in insufficiently washed or degraded samples (e.g. [Fig. 7C](#) and [D](#) showing the thawed sample).

[Fig. 6](#) presents scatterplots of blood, blood plasma and isolate prepared from fresh blood sample following the protocol #1 ([Table 1](#)). Regions were determined based on preliminary tests with washed erythrocytes and samples labeled with cell-specific markers. After removal of cells (by centrifugation of blood at 2 000 g and 22 °C for 30 min), the blood plasma was rich with particles in the size range of platelets and smaller (concentration of all detected particles in cell-depleted plasma was 49 200/ $\mu\text{L}$  with 45% of those pertaining to the platelet region – central square gate in [Fig. 6B](#)). The scatterplot ([Fig. 6C](#)) corresponds to the isolate (concentration of detected particles was 19 620/ $\mu\text{L}$  with 95% pertaining to the platelet region). According to the FCM and SEM analysis, in protocol #1 ([Table 1](#)), the majority of the platelets that remained in the supernatant after centrifugation of blood at 2 000 g, were sedimented after the first centrifugation at 17 570 g, 20 min, 22 °C. It can be noted (see the scatterplots in [Fig. 6](#)) that the source blood plasma contained higher amount of particles smaller than 500 nm (the size was estimated by FCM analysis of standard polystyrene beads) than the isolate, meaning that those particles (found in supernatant [Fig. 5](#)) were largely removed in the washing steps of isolation.

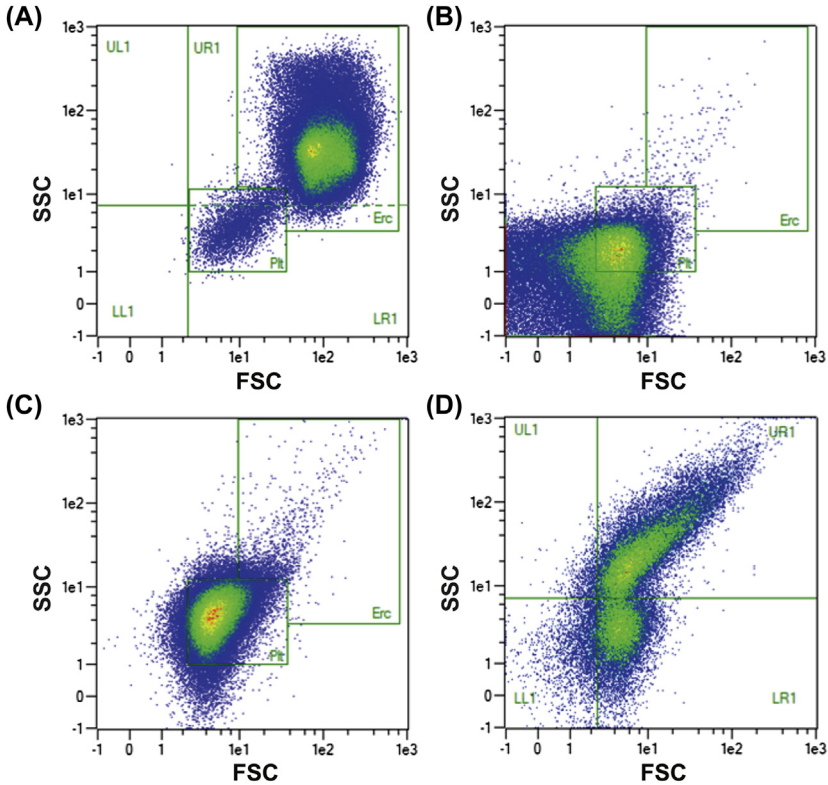


**Fig. 6** Flow cytometer scatter plots of: (A) blood; (B) supernatant after centrifugation of blood at 2 000 g, 22 °C for 30 min – blood plasma; (C) isolate obtained by protocol #1 (17 570 g, at 22 °C for 20 min, [Table 1](#)); (D) thawed plasma sample, used in protocols #1a,b-#10, [Table 1](#). Gates were set based on preliminary study (not shown). Well defined populations of erythrocytes (Erc) and platelets (Plt) can be seen (marked as Erc and Plt in Panels A–C, respectively). Leukocytes appear in the Erc gate, but in case of whole blood, their contribution to the count in this gate is negligible. Comparison of Panels B and D indicates that populations in thawed plasma sample are different from populations in fresh plasma. Populations in 4 quadrants in Panel D were defined for the convenience of the analysis: large and strongly scattering particles (UR1), large and weakly scattering particles (LR1), small and strongly scattering particles (UL1); small and weakly scattering particles (LL1). For comparison, those gates are also represented on the sample of blood (Panel A). Population detected in the plasma (B) was open-spread to small and weakly scattering events (left and below from the platelet gate, respectively). Isolate (C) appeared as a closed population with majority of particles being larger than the lower detection limit of the flow cytometer (about 400 nm).

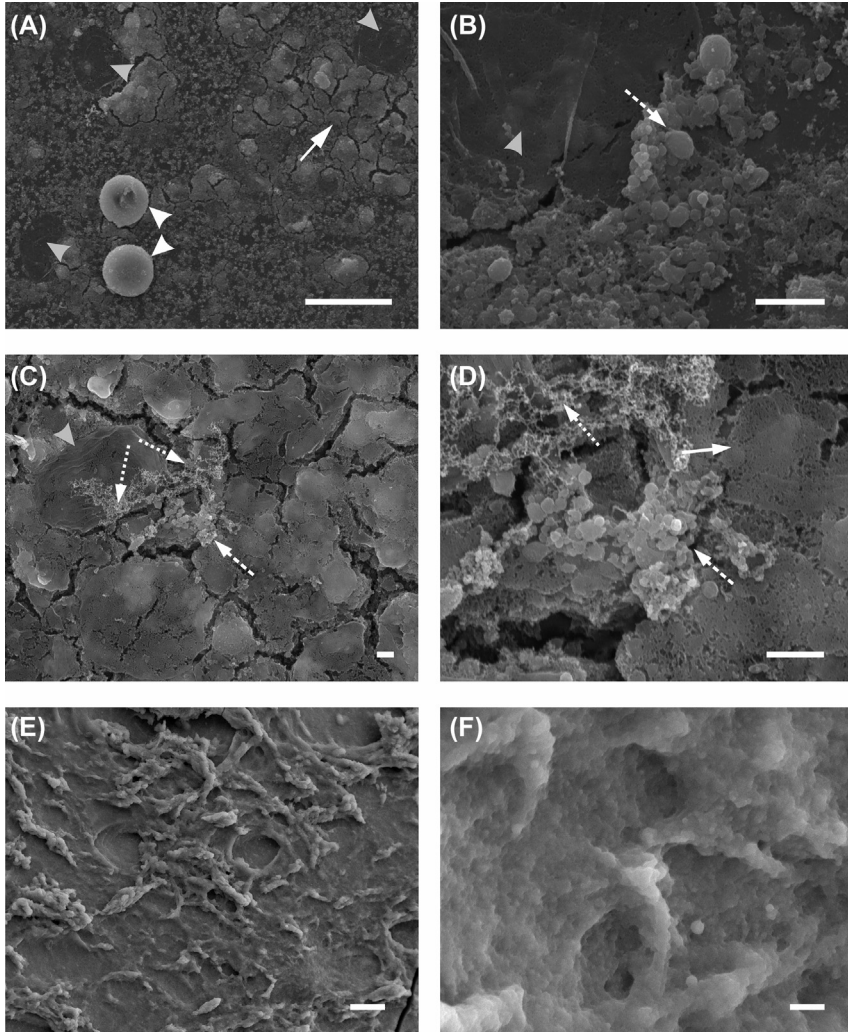
### 3.2 Parallel centrifugation experiment

Fig. 7 shows SEM images of isolates from thawed plasma obtained by parallel centrifugation at different centrifugation speeds, i.e.: at 10 000 g at 8 °C (Fig. 7A and a close up on Fig. 7B, protocol #2, Table 1), at 17 570 g and 22 °C (Fig. 7C and A close up on 7D, protocol #1a, Table 1), and the surface of a pellet after 8 h centrifugation at 100 000 g, 22 °C (Fig. 7E and A close up on 7F, protocol #5, Table 1). Singular relatively intact residual erythrocytes (marked by white arrowheads) and traces of erythrocyte ghosts (marked by gray arrowheads) can be observed in the isolates obtained by lower centrifugation speed 10 000 g (Panel A). Isolates obtained by higher speeds (Panels B–D) yielded sub-micron particles (marked by dashed arrows in Panels B, C and D) and coalesced precipitates (marked by dotted arrows in Panels C and D). However, none of these particles attained a characteristic EV shape corresponding to the minimum of membrane free energy (such as ones found in isolates from fresh plasma, Fig. 3D). We could not distinguish particles in the material obtained by 8 h centrifugation at 100 000 g (Panels E and F).

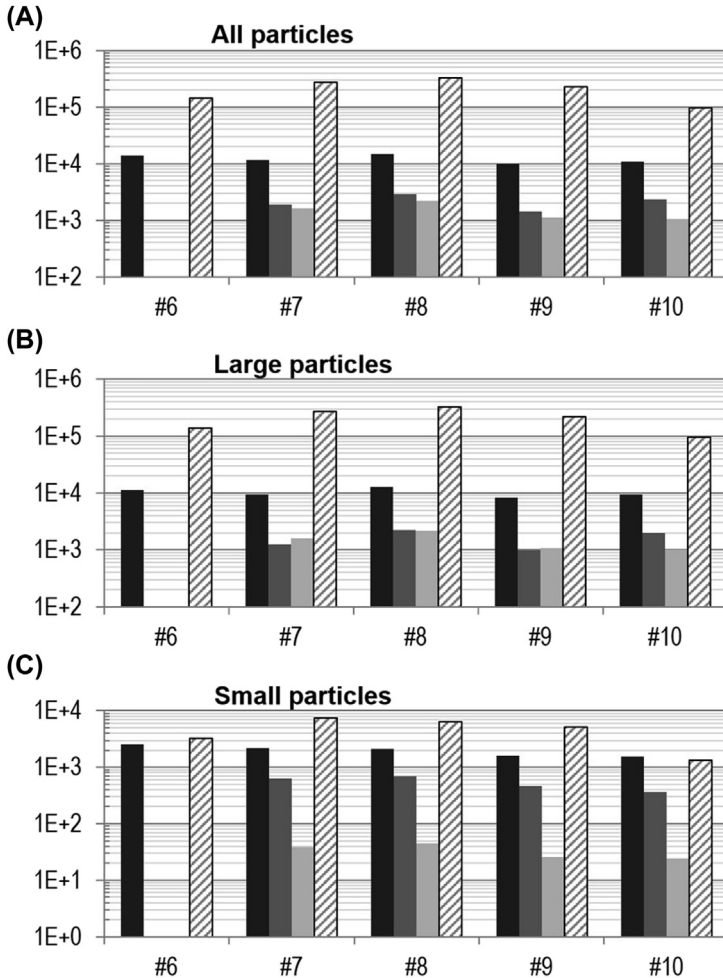
The number of events in plasma and in isolates from plasma obtained by protocols #6–10 (Table 1) was assessed by FCM (the results are given in Table A1 and Fig. A3 in the Appendix). The gates for FCM analysis of thawed-plasma derived samples were set based on preliminary study and SEM analysis (Fig. 7). The events were divided among 4 quadrants (shown in previous subchapter, Fig. 6D and in Appendix, Figs. A1–A2, A5); upper-right (UR): residual erythrocytes, cell ghosts (wide arrowheads on Fig. 7), and large aggregates; lower-right (LR): fragmented cells (full line arrows in Fig. 7); lower-left (LL): small and weaker side-scattering particles; upper-left (UL): small but stronger side-scattering particles). For analysis convenience, events were divided between larger particles (right regions: cell residual) and smaller particles (left regions).

Fig. 8 shows FCM records on the number of total events (A) and in of events recorded in the gates where we expect residual cells and cell debris (B), and smaller particles (C). Results on parallel centrifugation at increasing centrifugation speeds are shown. The number of events in the gates where we expect residual cells fluctuated for about 25% in source plasma (black bars in Fig. 8B) which estimates of the FCM measurements.

The number of events was higher in isolates than in other samples. The number of events was higher in plasma than in supernatants, but the clearance of particles was not directly related to applied centrifugation speed. No



**Fig. 7** Scanning electron microscopy images of isolates obtained by centrifugation at 10 000 g at 8 °C (A and a close up in B, protocol #2, [Table 1](#)), at 17 570 g and 22 °C (C and a close up in D, protocol #1a, [Table 1](#)), and the surface of a pellet after 8 h centrifugation at 100 000 g (E, and a close up in F (protocol #5, [Table 1](#))). The wide arrowheads point to erythrocytes (white arrowheads) and erythrocyte ghosts (emptied cell membranes, gray arrowheads). Full-line arrows indicate platelet remains (degraded deposits of aggregated cells), dashed arrows point to sub-micron-sized particles (EVs), while dotted arrows in Panels B–D point to nets of small globular particles, presumably precipitates of proteins. Material in pellet obtained after 8-h centrifugation at 100 000 g was of inrecognizable structure (pannels E, F). Scale bars: 10  $\mu\text{m}$  in (A), and (E), 1  $\mu\text{m}$  in (B), (C), (D) and (F).



**Fig. 8** Concentration of particles in samples from plasma, isolation supernatants and isolates as measured by flow cytometry. We compared protocols #6–10 (Table 1) presenting increasing speed of parallel centrifugation (#6: 10 000 g, 1 h, #7: 20 000 g, 1 h, #8: 50 000 g, 1 h, #9: 100 000 g, 1 h, #10: 100 000 g, 2 h). Events detected by FCM (A) were divided with respect to their FCS signal, which is proportional for the particle size. Changes in larger particles' concentrations are represented in graph B and those in smaller particles in Panel C. Supernatants of the sample processed by protocol #6 have not been measured due to technical problems. Black – source plasma samples; dark gray – first supernatant; light gray – second supernatant (washing step); stripped bars – isolate.

trend was observed in the number of events corresponding to platelets and larger fragments in the supernatants with increasing centrifugal pull. The number of events corresponding to larger particles was higher than the number of events corresponding to smaller particles in all samples (see that the scales in panels A and B differ by 2 orders of magnitude). Interestingly, the number of larger particles was almost the same in the two supernatants (Fig. 8B) while the number of smaller particles (EVs) was smaller in the second supernatant (Fig. 8C). This indicates that larger fragments were pelleted in both centrifugation steps while some smaller ones were lost in the first step of isolation (plasma centrifugation).

The respective number of events corresponding to both, larger and smaller particles in isolates, increased with enhanced centrifugal pull and reached a maximum at 50 000 g (Fig. 8A–C). With continuing increase of the pull, the number of events then decreased at 100 000 g, 1 h (protocol #9) and further dropped at extended duration of UC at 100 000 g, 2 h (protocol #10).

In the first and second supernatant there was an interesting inversion of the ratio between weaker and stronger side-scattering particles (Appendix, Fig. A4). In the first supernatant there was a larger share of weaker side-scattering particles, while in the second supernatant, strongly side-scattering particles represented a vast majority in all samples. It seems that some particles are eliminated with the supernatant based on their buoyancy (density and shape).

As by the FCM small and large particle concentration appeared proportional to each other, the possible hidden differences in smaller particles were assessed by DLS analysis.

The results of DLS analysis of the isolates and their corresponding plasma supernatants after the first step of isolation (high speed centrifugation) are given in Appendix (Table A2). Note, that the size parameters obtained by DLS should not be taken as direct dimensions of the particles, rather they must be considered with respect to particle's scattering properties. Furthermore, the width of a peak (dispersion of particle sizes around the determined mean size) should be taken into account as well.

The size distribution of particles in the isolates in comparison to plasma sample and supernatants showed similar trend in all samples. In Fig. 2 (in the Experimental section), prevalence of smaller particles ( $R_h < 50$  nm) in plasma supernatant over those in the isolate can be observed. This is expected, as free plasma proteins ( $R_h < 10$  nm) are presumed to remain in the supernatant, and the isolate is supposed to be further cleared of them

in the washing step(s). The peaks with mean  $R_h$  10–500 nm were in focus in this study, as they are presumed to carry information about vesicles (peaks with  $R_h$  10–200 nm) and cell debris (peaks with  $R_h$  200–400 nm, particles assessed by FCM, Fig. 8). The intensity of scattered light was determined for each separate peak. Intensities of the peaks with  $R_h \leq 1000$  nm were counted-up and their contribution to the total measured intensity was calculated (the results are given in Table A2). The smaller contribution of particles with  $R_h > 1000$  nm to the total scattered light intensity in the isolates prepared with higher centrifugation speeds therefore indicates the higher presence of large aggregates ( $R_h < 5 \mu\text{m}$ ) in them.

Fig. 9 shows the intensity of scattered light measured by DLS analysis and concentration of particles assessed by FCM. As the trends were similar for the peaks of smaller particles (with mean  $R_h$  (10–100) nm, and for the larger particles with mean  $R_h$  (100–500) nm; the collective intensity of scattered light for all the particles with  $R_h \leq 1000$  nm is therefore shown in Fig. 9 ( $I_{R_h \leq 1000} = \int_{R_h=0}^{R_h=1000} I(R_h) dR_h$ , gray bars). Stronger scattering was detected in samples with higher concentration of particles determined by FCM (see the correspondence of DLS and FCM results presented in Fig. 9 by gray and black bars). Because the large particles scatter light much stronger than the small ones, and because the particles detected by FCM are included in the populations assessed by DLS, this agreement of

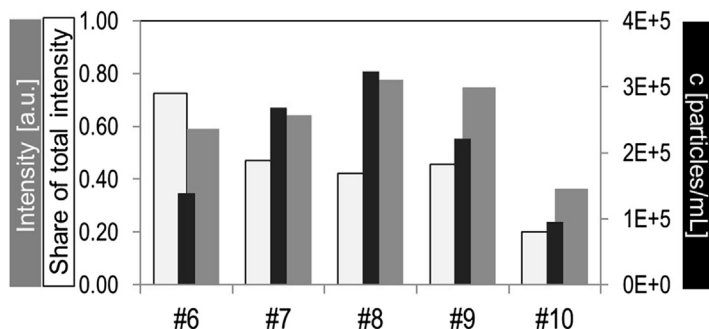


**Fig. 9** Comparison of dynamic light scattering (white gray and gray bars) and flow cytometry results (black bars) for isolates obtained by protocols #6–10 (Table 1, increasing centrifuge speeds from 10 000–100 000 g at 8 °C). The intensity of scattered light was determined for each separate peak ( $I_{R_h}$ ). Intensity of peaks with  $R_h \leq 1000$  nm was summed-up ( $I_{R_h \leq 1000} = \int_{R_h=0}^{R_h=1000} I(R_h) dR_h$ , gray bars) and their relative contribution to the total measured intensity was calculated (fraction of intensities  $I_{R_h \leq 1000}/I_{total}$ , white bars). Concentration of all detected particles by FCM is demonstrated by black bars. a.u. – arbitrary units; c – concentration;  $R_h$  – hydrodynamic radius.

results is expected. On the other hand, this correlation indicates that more severely processed samples did not contain larger amounts of small particles, which are below the detection limit of FCM, but can be detected by DLS. The decrease in the contribution to the total intensity of scattered light attributed to the particles with  $R_h \leq 1000$  nm (fraction of intensities  $I_{R_h < 1000} / I_{total}$ , presented in Fig. 9 by white bars) rather suggests that increasing forces at higher centrifugation speeds cause particle aggregation. Larger particles scatter light much stronger than the small ones, and therefore, even very few aggregates (particles  $R_h > 5 \mu\text{m}$ ) that are present in the sample strongly lower the contribution of smaller particles ( $R_h \leq 1000$  nm) to the total intensity. In contrast, very large particles may be excluded from FCM detection as they exceed the detection range determined by the settings, or if these particles are associates of many, they might dissociate in the flow before the detection.

FCM displayed a trend in the change of side scattering properties of particles with increasing centrifugation pull. While there was little or no change detected in the forward scattering signal (Fig. 10A–E, K–O), the side scattering of the particles in the isolate became stronger with the increase in the centrifugation pull (see the SSC scatterplots in Fig. 10F–J, P–T). The single peak with relatively low SSC gradually broadened toward right (Fig. 10F–J) and split at higher forces (protocol #10, centrifugation at 100 000 g, 2 h, 8 °C, Fig. 10P). This trend was further amplified when centrifugation was performed at higher temperature. The peak with higher SSC enhanced and prevailed in protocols #2–4 (1 h centrifugation at 22 °C at 10 000 g, 20 000 g, and 100 000 g, respectively; Fig. 10Q–S), and finally disappeared in the isolate of protocol #5 (8 h centrifugation at 100 000 g, 22 °C; Fig. 10T). In the sample processed for 8 h, the drop in the scattering intensity (shift of FSC and SSC distributions to the left, Fig. 10O and T) suggests degradation of the sample.

### 3.2.1 Analysis of the changes in protein profiles

The concentrations of proteins in the isolates obtained by the protocols #1a–5 (from the same blood plasma sample) determined by the BCA method were 2.30 (isolate #1a), 4.01 (isolate #2), 17.22 (isolate #3), 15.55 (isolate #4) and 101.08 mg/mL (isolate #5). The SDS-PAGE image of their protein profiles (20  $\mu\text{g}$  proteins) is shown in Fig. 11.

The overall protein profiles of the various isolates are very similar and characterized only with slight expression differences. Some well-resolved bands were selected for MS-based proteomic analysis as shown in Fig. 11.

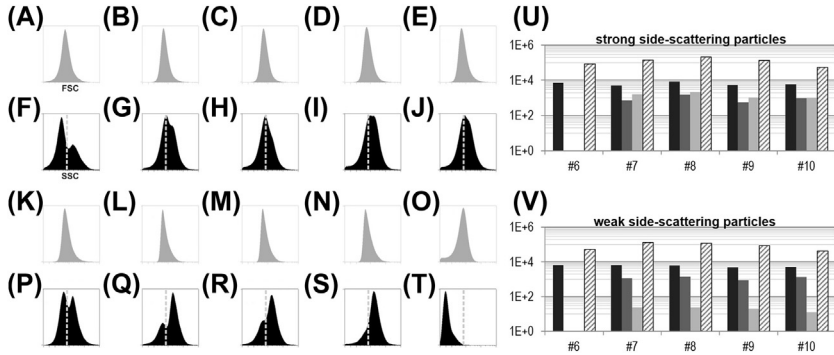


**Fig. 10** Forward (gray) and side scattering distributions (black) of particles in the source plasma sample and in the isolates obtained by centrifugation at different centrifugation speeds at 8 °C (protocols #6–10, [Table 1](#)) and at 22 °C (protocols #2–5, [Table 1](#)) as determined by FCM. Please note, that in protocols #2 and #6; #3 and #7; and #4 and #9, same speeds but different temperatures were applied. (A, F) a plasma sample; (B, G) isolate of protocol #6, centrifugation at 10 000 g, 1 h, at 8 °C; (C, H) isolate of protocol #7, centrifugation at 20 000 g, 1 h, at 8 °C; (D, I) isolate of protocol #8, centrifugation at 50 000 g, 1 h, at 8 °C; (E, J) isolate of protocol #9, centrifugation at 100 000 g, 1 h, 8 °C; (K, P) isolate of protocol #10, centrifugation at 100 000 g, 2 h, 8 °C; (L, Q) isolate of protocol #2, centrifugation at 10.000g, 1 h, 22 °C; (M, R) isolate of protocol #3, centrifugation at 20 000 g, 1 h, 22 °C; (N, S) isolate of protocol #4, centrifugation at 100 000 g, 1 h, 22 °C; (O, T) isolate of protocol #5, centrifugation at 100 000 g, 8 h, 22 °C. The plots are normalized to surface area = 1. A vertical guideline is added to the SSC plots F–J and P–T to highlight the trend of change in side-scattering properties of particles in the isolates obtained by different protocols in the presented order. Changes in concentration of strongly (U) and weakly (V) scattering particles throughout the processing by different protocols are also represented (supernatants of the sample processed by protocol #6 have not been measured due to technical problems). Black bars – source plasma samples; dark gray bars – first supernatant; light gray bars – second supernatant (washing step); striped bars – isolate.

The results of LC-MS/MS-based protein identification are shown in [Table 2](#). Proteins identified in the various samples are highly abundant human blood plasma proteins, as explained by Strohkamp et al. [63]. Proteins identified in bands 1–3, for example, were found to be progressively enriched in samples #2, #3 and #4 upon increasing centrifugal forces. By comparing the isolates prepared with different centrifugation speeds, we see accumulation of fibronectin (Band 2) with increasing force. Fibronectin was largely eliminated in the isolate #5. Protein(s) in Band 5 were highly enriched in the sample #4 (8 h centrifugation time) while Apolipoprotein-B-100 (Band 6) decreased with increased centrifugation speed. Other bands did not differ substantially in the different samples.

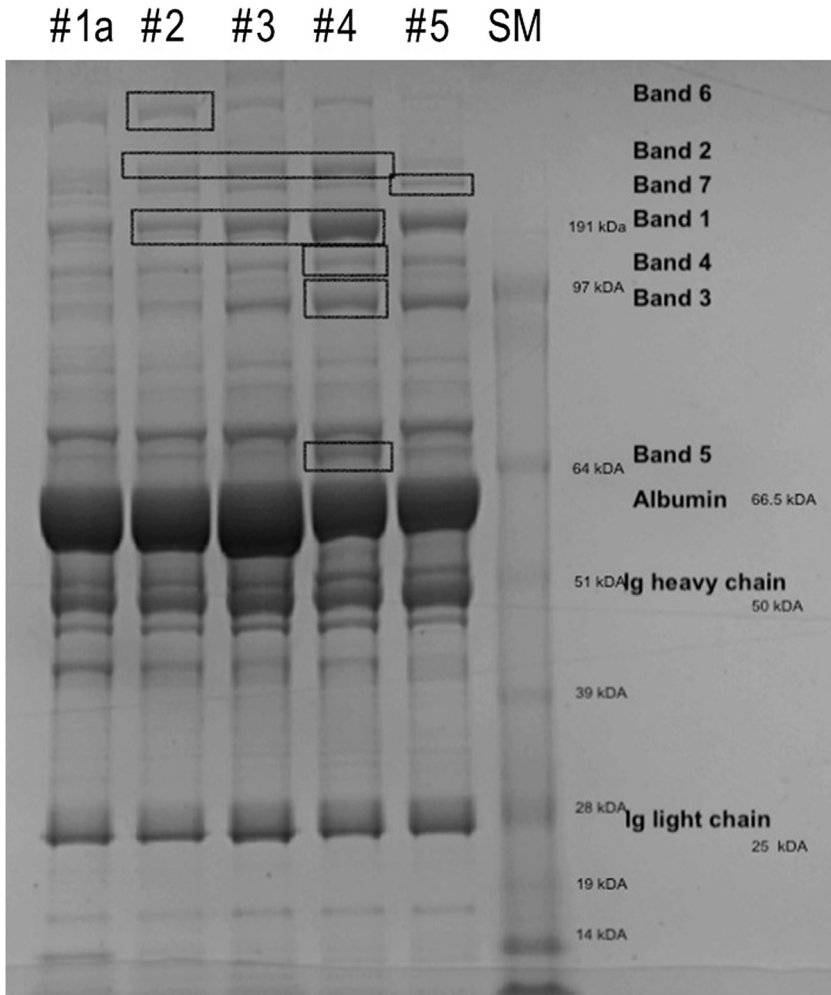
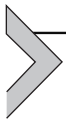


**Fig. 11** SDS-PAGE protein profiles of isolates obtained by protocols #1a-5 (different centrifugation times and speeds, performed at 22 °C) at reducing conditions. SM – size marker. Band selection for mass spectrometry analysis is noted by the frames. Bands 1 and 2 were taken from the isolate #4.



## 4. Discussion

### 4.1 Source of vesicles in the isolates

From a very basic perspective, two springs of EVs can be expected in biological samples – i) internal – cell-directed production of vesicles through controlled change of membrane components (including formation

**Table 2** Gel-based proteomics results. Proteins identified in isolates 1a-5 using different centrifugation regimes (protocols #1a-5). UniProt ID indicates the accession numbers from the UniProt database; Mascot ion scores indicate the scores obtained from the Mascot software. Identification of protein in previous proteomic research of EV isolates [64].

Band	UniProtID	Protein name	Molecular weight (kDa)	Score	Previously related to EVs
1	P01023	Alpha-2-macroglobulin	165	1287	[56–59]
2	P02751	Fibronectin	266	498	[56,59–61]
3	P01023	Alpha-2-macroglobulin	165	509	[56–59]
	P01024	Complement C3	189	302	[56,58,59]
	P02768	Serum albumin	71	80	[59]
4	P00450	Ceruloplasmin	123	121	[56,60,61]
	P01859	Immunoglobulin heavy constant gamma 2	37	71	[62]
5	P01871	Immunoglobulin heavy constant mu	50	443	[56,60,61]
	P01024	Complement C3	189	346	[56,58,59]
	P02768	Serum albumin	71	324	[56–61]
	P0C0L4	Complement C4-A	194	276	[56,59]
	P04003	C4b-binding protein alpha chain	68	120	[59]
6	P04114	Apolipoprotein B-100	517	495	[56]
7	P02751	Fibronectin	266	79	[56,59–61]
	P02768	Serum albumin	71	77	[56–61]
	P01023	Alpha-2-macroglobulin	165	69	[56–58]
	P02760	Protein AMBP	40	58	[56,59,60]

of so-called ectosomes, exosomes and apoptotic bodies); and ii) external — spontaneous vesiculation caused by membrane perturbations under the change of system conditions (mechanical stress, change of chemical environment, temperature, etc). Considering the external path of EV genesis, the amount of EVs in an isolate depends on the quantity of cells and their fragility; while in case of internal path, the amount of EVs is expected to reflect metabolic (including communication) activity of the cells in focus. The ratio between vesicles of a certain cell origins is presumed to be related to the abundance of the cell populations in the examined tissues/samples and their vesiculation-activity.

In case of blood, blood cells are subjected to various perturbing conditions from the sampling on, e.g. change in temperature, contact with exogenous surfaces, shear forces in the needle etc. All of those may contribute to cell fragmentation and activation. It was previously observed that large portion of vesicles isolated from blood is of the platelet and/or erythrocyte origin [65–70]. Erythrocytes are by far the most abundant cells in blood, high prevalence of vesicles of their origin is therefore expected in case of cell degradation. Platelets are second most abundant cells in blood. Further, they are prone to vesiculate, especially in the activated state [68,70,71]. If a sample contains cells [72], vesicle count depends on sample storage. The studies showed, that the amount of platelet-derived EVs greatly increased when samples with platelets were exposed to lower temperatures, which can be related to platelet activation [17,68,73].

In the isolation processing the particles move, and are exposed to shear stress, which also provokes vesiculation [17,43]. One very important factor in centrifuge processing is temperature. Besides possible cell activation, lower temperature increases the viscosity of the sample — altering sedimentation times of particles, increasing shear forces, and changing membrane mechanical properties [74,75].

Some cells remain in the supernatant after the first centrifugation step, and most of them are platelets (represented in the scatterplot in Fig. 6B, and Figs. 3 and 4). Platelets are the smallest blood cells, and upon activation, they get branched (see Figs. 3A or 4A), which contributes to their slower sedimentation rate. In the following steps of isolation, the retained cells are subjected to high-speed centrifugation (i.e. > 10 000 g). In our samples, majority of the residual platelets sediment at 17 570 g. Interestingly, the platelets in the pellet retained adhesive properties as they bound to glass in the process of preparation for imaging (Figs. 3A and 4A). The morphology of adherent platelets in the transferred samples (activated globular shapes

with tubular protrusions; Fig. 4A) may be induced by the action of shear forces during the processing, although similar morphology was reported in relation to their interaction with glass surface [76] or their late apoptotic state [77].

When cells and their fragments during centrifugation reach the tube wall the shear forces on them greatly increase. If the cells are fragile and their membranes are fluid enough to form vesicles after tearing, the vesicles are formed from damaged cells. This can result in high quantity of vesicles originating from cells that were not efficiently removed in the previous steps of isolation.

In the supernatant after centrifugation of fresh plasma at 17 570 g (protocol #1), fragments of membranes (arrowheads, Fig. 5) and some loose globular particles (full-line arrows, Fig. 5) splotching on the surface of the filter were noted. We speculate that they could be low density lipoproteins, lipid droplets or possibly some low density vesicles, formed after cell destruction and membrane phase separation. Such vesicles are not expected to sediment due to possible low density content, poor on proteins. However, those particles were not exhibiting predicted vesicle-shapes.

Microparticle formation upon shear stress was reported by many authors, e.g. Ref. [17,43,78–80]. Similarly to the previously published data [17,43], we found many vesicles attached to the surface of the centrifuge tube wall. Their shapes (see Panels B–D of Fig. 3) correspond to characteristic shapes calculated by the minimization of the membrane free energy [17,55], which indicates that they are without internal structure and fulfill the requirements for the definition of cellular vesicles. Tubular particles seemed to orientate according to the flow established during centrifugation (see Fig. 3C), and were likely formed due to shear forces. Similar platelet tethers related to shear stress were described by Reininger et al. [79]. Round vesicles can be formed later from such tubular remnants by “pearling” [79,81]. Indication of such proceeding is visible in Fig. 4 (see short-dashed and dotted arrow). As vesicle-like particles were found in high amounts only near the tube surface, we hypothesize that they were formed from the platelets in the high shear stress field near the centrifuge-tube wall. Large share of vesicles of platelet origin in isolates can therefore be ascribed to platelets’ proneness to form vesicles, and their lag behind in sedimentation, bound up to their later fragmentation in the subsequent processing. We assume that the observed structures found in the isolates by protocol #1 are representative also for other protocols considered (if fresh blood is used as a source

material), meaning that such particles, formed upon processing may overwhelm the isolates, claimed to be extracellular vesicles.

The isolation protocols yield material, which upon analysis (e.g. by light scattering and microscopic techniques) reveals presence of particles. The samples prepared from fresh and frozen/thawed blood plasma were analyzed in this study with the aim to better understand the origin of these particles found in the isolates. Thorough analysis of individual steps of the isolation protocols was performed. As EVs are too small to be observed by optical microscopy, the samples were imaged by scanning electron microscopy. Dynamic light scattering was employed to reveal the size distribution of particles, and flow cytometry was used to determine concentrations of particles larger than about 400 nm. In analysis of the isolate prepared from fresh plasma by a protocol commonly used in clinical studies [17,32–46] many activated platelets were observed in the sample mounted on holder, while the deposits of vesicles with characteristic shapes of minimal membrane free energy were found attached to the walls of the centrifuge tube in which the isolation was performed (Figs. 3 and 4). Present and previous studies indicate that these vesicles are formed by tearing and re-sealing of the residual cells in the samples (mostly erythrocytes and platelets). The present study provided further evidence that the isolates of a fresh plasma by the protocol that includes centrifuge centripetal accelerations up to about 20 000 g consist of a heterogeneous mixture of residual platelets and blood cell fragments.

Frozen/thawed samples were treated at different centrifugation speeds, including the one similar to the one used for the fresh sample (17 570 g/20 000 g), but also milder and harsher ones, in order to reach the renowned conditions for gathering the exosomes at around 100 000 g. It was found that all the isolates from frozen/thawed samples were substantially different from the isolates from fresh samples (compare Figs. 3, 4, and 7). The heterogeneous population of submicron-sized particles from frozen/thawed plasma observed in micrographs (Fig. 7) could not be recognized as a population of intact or even activated platelets; the shapes of observed particles were of irregular globules. Aggregates of nanoparticles were presumed to be protein precipitates (Fig. 7). No particles with characteristic shapes corresponding to the membrane free energy minimum that would comply to the definition of cellular membrane vesicles (membrane enclosed entities without internal structure, such as the ones evident in Fig. 3D in fresh

plasma) were found in the samples from thawed plasma. We suggest that the majority of particles found in the isolates of frozen/thawed plasma are residual platelets that deformed and/or fragmented due to thermal and mechanical stress imposed upon them in the process of isolation. Both techniques, FCM and DLS detected particles in the isolates. There was an agreement of the estimated concentration of particles trend detected by these two techniques (Fig. 9) showing that the concentration of particles in the isolates varied with changing the parameters of processing (the centrifuge centripetal acceleration). These results provide further evidence in favor of the hypothesis that majority of the isolated particles are fragments of residual cells in samples. Most importantly, DLS measurements have shown differences in size distribution and amount of particles with hydrodynamic radii smaller than 1  $\mu\text{m}$  with different centrifugation pull (Appendix Table A2) that were not correlated to the clearance of same sized particles from the sample supernatant. This indicates that the small particles in the range of expected “exosomes” may be created in the process of isolation.

We failed to observe EVs in the exosome size range in the SEM images of the thawed samples. However, we also did not succeed to observe larger EVs when the isolate was transferred for imaging on a filter paper or on glass (Fig. 4) and there is a possibility that smaller particles were lost during mounting of the sample on the stands for SEM. Further improvement of sample preparation is necessary to give a decisive answer on the question whether the EVs with characteristic shapes of membrane-enclosed entities smaller than 100 nm are present in the isolates from human blood plasma with the protocols for harvesting exosomes.

These observations provide important knowledge as regards DC protocols and size and shape of vesicles. Commonly, the strategy for larger vesicles harvesting is application of lower centrifugation speed, while higher speeds (and forces) are applied for isolation of smaller vesicles [82]. This seems rational according to the sedimentation theory, but considering shear-induced tearing, it is also expected that stronger forces, will cause stronger grinding and that the size of particles (obtained from the same starting material) will therefore depend on centrifugation speed and time. The FCM analysis in this study shows that the material is being transformed throughout the centrifugation processing. One can observe the change of populations which correlate with constraining of the applied conditions (first increase of speed and later increase in temperature). While hardly any change can

be observed in FSC, the differences in SSC properties of the particles in the samples are apparent. We could not attribute this distribution shift to the additional (smaller and lighter) particles being pelleted in samples of enhanced UC procedure. It therefore seems that it is related to the transformation of material upon processing. The stronger scattering particles appeared to be more stable, and were even further produced along the sample storage (see Appendix; Fig. A5).

## 4.2 Isolation efficiency

Understanding of sedimentation is crucial for efficient isolation of vesicles by DC. The properties of vesicles and the medium must be considered in the protocol design. The sedimentation rate of particles depends on their density, size and shape, and the viscosity of medium they are passing. During the centrifugation, components of the sample arrange/separate due to centrifugal forces and establish a density gradient. Particles travel until the equilibrium state is established (sedimentation limit is reached when the particles are distributed by their density).

Although the increase of speed and time of centrifugation reinforce the efficiency of sedimentation, long time/high speed centrifugation may cause vesicle degradation [12,25,26]. Our experiments suggest that redistribution of lipids and proteins may occur in prolonged UC. The particles in our samples lost their optical density after centrifugation at 100 000 g for 8 h (see Fig. 10T). The nucleic acids and proteins may severely precipitate at such extreme conditions and form a gelatinous precipitate.

Temperature is a very important factor in EV isolation processing. As long as the cells are present in the sample, the change in temperature may induce their activation. On the other hand, it also strongly affects medium viscosity, and mechanical properties of sample components. Medium viscosity is lower at higher temperature; the sedimentation is faster and its limit is reached sooner. While lower temperatures are expected to preserve proteins and make membranes more rigid, there are indications that loss of cell membrane fluidity, makes it more susceptible to mechanical damage [83]. Furthermore, shear forces which are key in fragmentation of cells in the centrifuge are higher at lower temperatures.

Cell fragmentation is considered as an artifact in isolation protocols. To avoid cell fragmentation, it is recommended to remove the cells and large particles in several low-speed steps [15]. However, when the supernatant

is transferred, some vesicles from the sample are lost due to their adhesion to the surfaces of the centrifuge tube and pipette tips. These losses depend on the composition and properties of the membranes as well as on the properties of the material composing laboratory equipment. Therefore, the procedure and materials used may also modify the populations of vesicles in the final isolate. In our study, microvesicles were found to stick quite strongly to the polypropylene surface, and were largely missing in the transferred sample (represented on Fig. 3 of the isolate in the tube, and Fig. 4 of the isolate fixed on cover glass).

### 4.3 Identity of particles in EV isolates (EVs' genuineness)

Finding specific vesicle markers is challenging because, regardless of them being intact or re-formed, the vesicle membrane retain the membrane associated proteins. It is an essential task to evolve purification to ensure that free proteins, nucleic acids etc. acquired during the processing do not shade those which are innately integrated-in or exposed-on EVs.

From Fig. 11, it is clearly apparent that the protein profiles of all our samples were very similar to that of starting whole plasma sample. The protein concentration of isolates was consistent with the concentration of the particles determined by FCM, while DLS has shown that small particles (with  $R_h < 15$  nm) were much more abundant in the supernatant fractions than in the isolates. These observations suggest that a large portion of proteins in these isolates is a part of supramolecular assemblies, rather than dissolved as single particles alone.

The amount of apolipoprotein B-100 (APOB, band 6) was found to be decreased in the isolates prepared with increased time of ultracentrifugation. Accounting APOB inclusion in low density lipoproteins (chylomicrons, VLDL and LDL), it is expected to accumulate in the top layers of the supernatant. The efficiency of APOB removal is therefore correlated with the establishment of the density gradient in the sample upon UC.

Alpha-2-macroglobulin (A2MG, bands 1 and 3) was found to be enriched in pellet fraction proportionally to the keener conditions. A2MG is known to display different SDS-PAGE bands under reduced conditions; moreover, it is sensitive to freezing and can be degraded during sample processing. The increased intensity of band 1 could be due to UC related efficiency of sedimentation which is in-turn associated with enhanced protein degradation.

Fibronectin (FINC, band 2) was enriched in the isolates of protocols #1a–4. Activation of hemostasis system can induce fibronectin binding to platelets [84,85] and may therefore sediment with membrane particles. On the other hand it is known that shear stress can induce its unfolding and polymerization [86,87]. It is therefore probable, that in the isolate #5, the fibronectin was a part of gelatinous pellet and largely excluded from the isolate.

Band 5 was disproportionately augmented in the isolate of protocol #4. It was found to contain several proteins that are associated with immune system activation, namely labeling of damaged material for clearance. Other bands did not differ substantially in different samples.

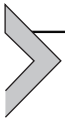
All the identified proteins of the isolates obtained in protocols #2–4 were previously associated with EVs, blood derived microparticles, or cell membranes (the associations denoted in Ref. [64] are summarized in Table A3). It is generally known that various “contaminants” such as non-EV proteins are found in EV isolates, and it was also seen that EVs isolated by UC are associated with a substantial amounts of albumin and other plasma proteins [56–61,88].

There are various possible causes for specific plasma proteins to be enriched in the pellet fraction (isolate) besides being a genuine constituent of EVs. For example, some proteins or protein aggregates can (a) sediment due to their size, shape and density, (b) form complexes with higher sedimentation rate, (c) bind to cell membranes and sediment together with them; (d) get enclosed into the cell fragments, formed upon cell mincing during processing. Whether the presence of those proteins in EV isolates is a feature of impurity of the sample or innate is yet to be clarified. The latter would mean that we may need to change our conception of “free” (soluble) plasma proteins.

We suppose that certain protein enrichment in isolates can be a result of up-taking surrounding components after reformation of the disrupted membranes. It was previously reported that plasma microparticles are hardly cleaned of [21] or bind [89] fibrinogen; which might be related to shear stress-induced vesicle formation and fibrinogen adhesive conformation change [90]. EVs are also frequently reported to expose phosphatidylserine (PS) [15,91] and bind complement system [92], as was also found in our samples. This is intuitively contradictory for particles striving long-distance reach, as such particles are expected to be quickly discarded by the macrophages [72,93]. Yet, PS is one of the generally accepted EV markers [15,91], and little was considered about such particles being a side product of

isolation. Arraud et al. [66] on the other hand showed that not all vesicles in blood plasma expose PS, and suggested that vesicles exposing PS are either formed by cell rupture or degradation, and subjected to the loss of membrane asymmetry.

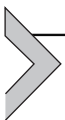
Our results show that vesicles formed in fresh plasma during processing have characteristic shapes which are usually non-spherical (see Fig. 3). Also, there seems to be a certain type of optically dense particles (strong side scattering) that can be produced during centrifugation (see Fig. 10) and sample storage (Appendix, Fig. A5), that are far more stable than others, and are therefore expected to be found in majority of the non-fresh blood derived EVs samples.



---

## 5. Conclusions

Better understanding of EVs' physicochemical properties is needed to further reveal their biology and exploitation of their potentials. In light of the hardly awaited break-through of extracellular vesicles from “could be used as” to “are successfully used in/as/for”, we here discoursed some factors hindering the progress in consideration of centrifuge-based isolation protocols. It seems that reporting observations is no longer enough, and further progress demands that we weight up what those observations mean. The close inspection of centrifugation processing in this study implies that starting material is easily transformed. While temperature, shear, and pressure play important parts in processing, uniqueness of starting samples defines the resulting isolate. This work 94 provided evidence that the majority of particles found in isolates from blood plasma are fragmented blood cells, mostly platelets whereby fragmentation takes place due to thermal and mechanical stress during processing. Freezing/thawing of samples made essential changes to the isolate. Efficiency of isolation was found to reach a plateau between centrifuge accelerations between 50 000 g and 100 000 g. Prolonged centrifugation at 100 000 g was found to cause aggregation and degradation of material. Further and more detailed analysis is in progress [94].



---

## 6. Appendix

### 6.1 Flow cytometry

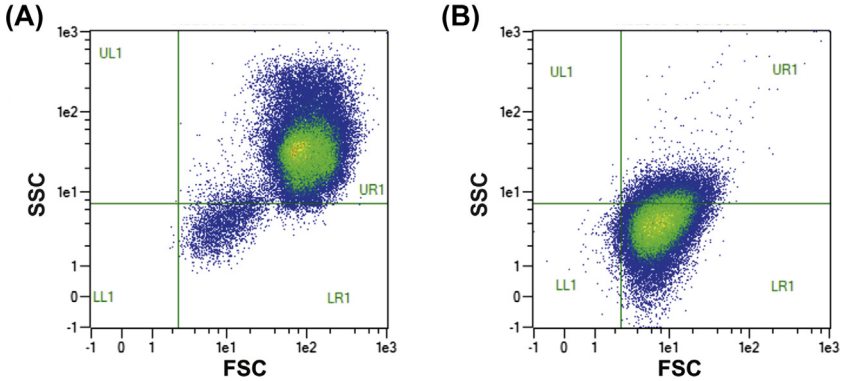


**Fig. A1** Examples of events corresponding to cells and particles in fresh blood (A) and in the platelet-rich plasma (B) prepared from it. Events corresponding to the erythrocytes, leukocytes and cell debris are found in the upper-right region (UR1) of the FSC-SSC scatterplot, while majority of platelets appear in the lower-right (LR1) region. The left two quadrants (UL1 and LL1) represent smaller and weaker-scattering particles, respectively.

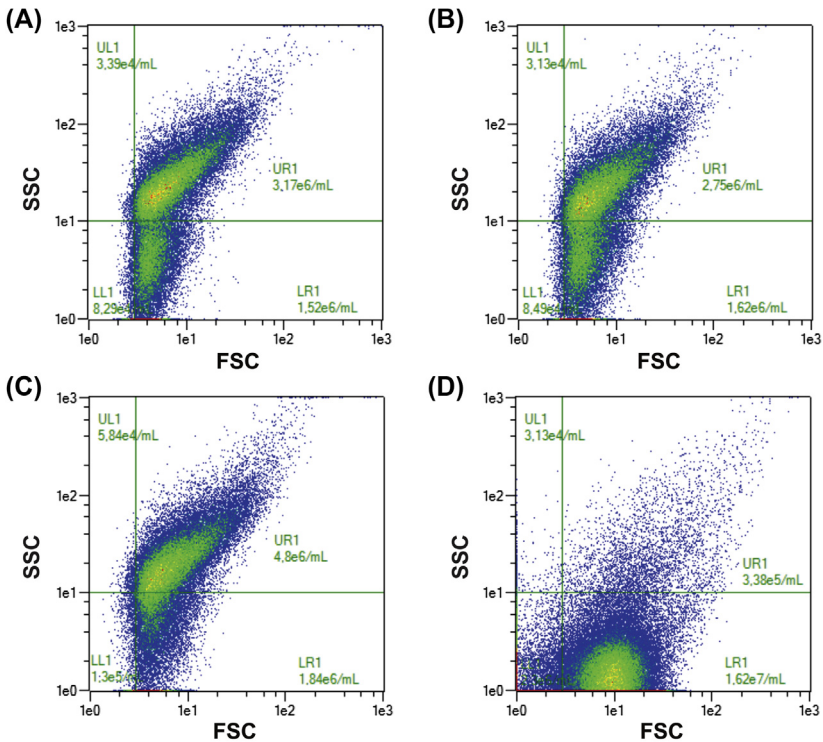


**Fig. A2** Examples of FSC-SSC scatterplots pertaining to the EV isolates from a frozen/thawed plasma sample, centrifuged at  $22^\circ\text{C}$ : (A)  $10\,000\text{ g}$ ,  $22^\circ\text{C}$  for 1 h (isolate #2); (B)  $20\,000\text{ g}$  at  $22^\circ\text{C}$  for 1 h (isolate #3); (C)  $100\,000\text{ g}$  at  $22^\circ\text{C}$  for 1 h (isolate #4) and (D)  $100\,000\text{ g}$  at  $22^\circ\text{C}$  for 8 h (isolate #5).

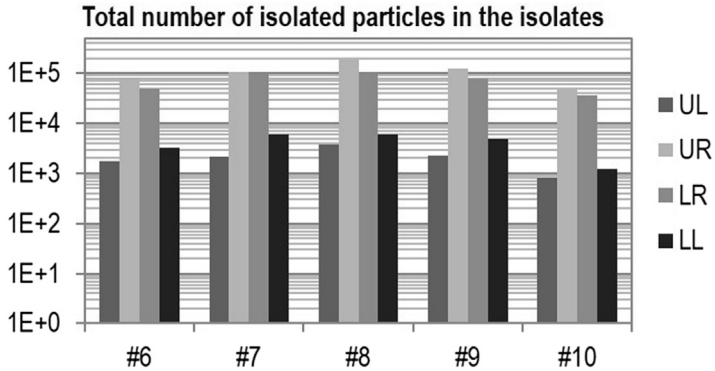


**Fig. A3** Comparison of particles in different gates in isolates #6–10. UR, large and strongly scattering particles; UR – large and weakly scattering particles; UL – small and strongly scattering particles; LL – small and weakly scattering particles.

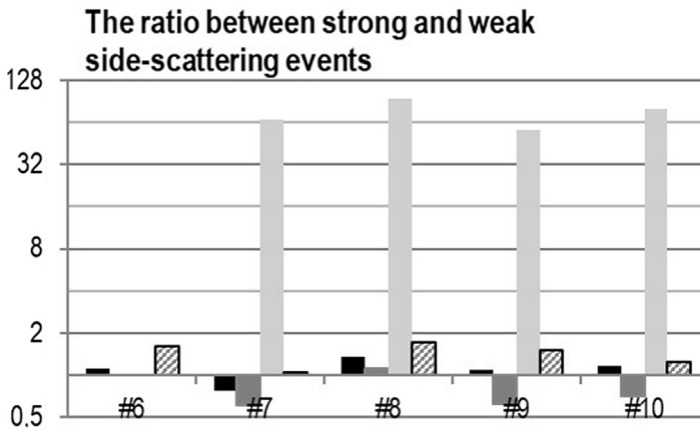


**Fig. A4** Comparison of the ratios of strongly and weakly scattering particles in the samples obtained in the processing according to isolation protocols #6–10. Black bars – source plasma samples; dark gray bars – first supernatant; light gray bars – second supernatant (washing step); stripped bars – isolate.

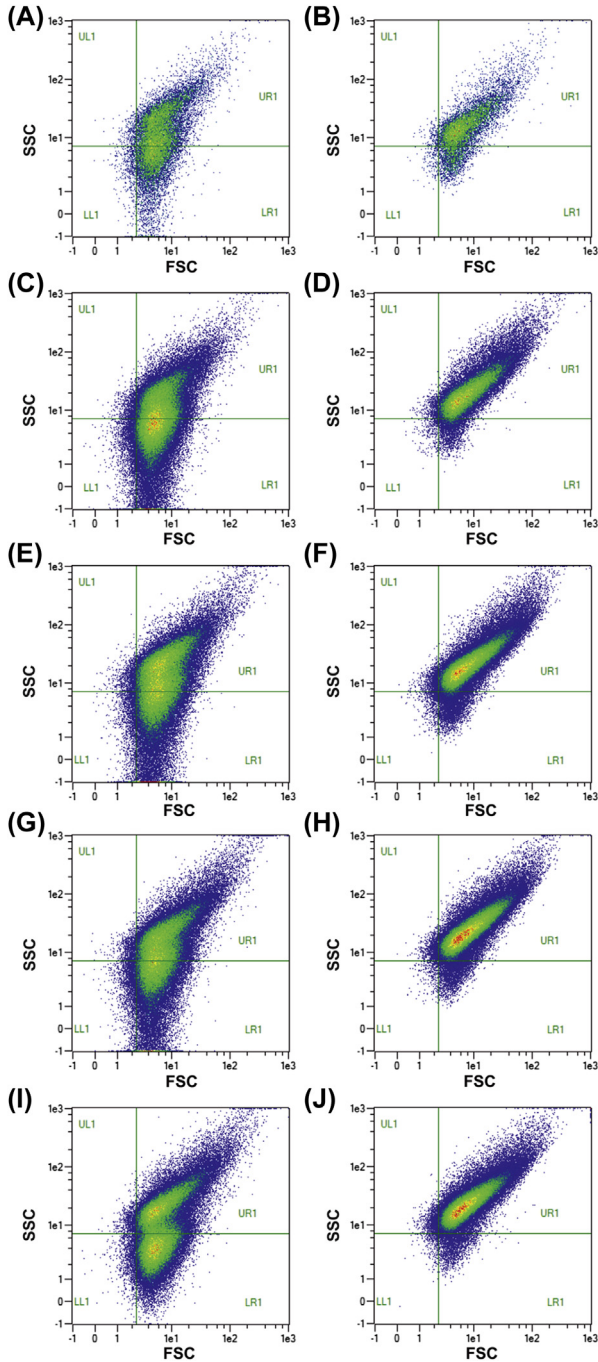


**Fig. A5** Isolates from a frozen/thawed blood plasma measured on the day of preparation (left side panels, A,C,E,G, I) and the same samples that were frozen at  $-80^{\circ}\text{C}$ , thawed, and then stored for a week at  $4^{\circ}\text{C}$  (right side panels; B, D, F, H, J). A,B, isolate #6; C, D, isolate #7; E, F, isolate #8; G, H, isolate #9; I, J, isolate #10.

**Table A1** Absolute concentration of particles isolated from frozen/thawed plasma in the second experiment of centrifugation (at 8 °C).

Protocol	RCF	Duration	Temperature	Total number of isolated particles <sup>a</sup>
#6	10 000 g	60 min	8 °C	1.39E+05
#7	20 000 g	60 min	8 °C	2.68E+05
#8	50 000 g	60 min	8 °C	3.23E+05
#9	100 000 g	60 min	8 °C	2.21E+05
#10	100 000 g	120 min	8 °C	9.01E+04

RCF, relative centrifugal force.

<sup>a</sup>Calculated from concentration obtained by FCM and sample volumes.

**Table A2** DLS results of isolates and their corresponding supernatants prepared from frozen/thawed plasma sample; obtained by protocols #6-#10.

isolate #6									
20 000g	dilution:		1:20						
Laser Intensity:	1.31E+01 mW								
Average Intensity I:	4.08E+01 kHz/mW								
Peaks	from t	to t	Mean t, s	Mean Rh, nm	mean G, s-1	mean D, cm2s-1	I, kHz/mW	I, % partel <1000nm	
1	1.20E-05	1.20E-05	1.20E-05	1	8.33E+04	2.39E-06	0.05	1	
2	5.97E-05	5.97E-05	5.97E-05	5	1.68E+04	4.80E-07	0.03	2	
3	6.61E-04	8.64E-04	7.54E-04	64	1.33E+03	3.80E-08	5.93	3	
4	3.29E-03	5.61E-03	4.75E-03	407	2.10E+02	6.03E-09	23.55	4	
5	5.85E+00	5.85E+00	5.85E+00	>1000	1.71E-01	4.90E-12	11.27	5	
sum I, partel Rh<1000nm							29.57		
estimated total I, partel Rh<1000nm							591.30		
Isolate #7									
20 000g	dilution:		1:20						
Laser Intensity:	4.60E+00 mW								
Average Intensity I:	6.85E+01 kHz/mW								
Peaks	from t	to t	Mean t, s	Mean Rh, nm	mean G, s-1	mean D, cm2s-1	I, kHz/mW	I, % partel <1000nm	
1	1.20E-05	1.20E-05	1.20E-05	1	8.33E+04	2.39E-06	0.04	0%	
2	5.70E-04	7.15E-04	5.90E-04	51	1.70E+03	4.86E-08	7.42	23%	
3	2.79E-03	3.50E-03	3.07E-03	264	3.25E+02	9.33E-09	24.67	77%	
4	8.15E-01	8.15E-01	8.15E-01	>1000	1.23E+00	3.52E-11	36.36		
sum I, partel Rh<1000nm							32.13		
estimated total I, partel Rh<1000nm							642.57		
Isolate #8									
50 000g	dilution:		1:20						
Laser Intensity:	3.57E+00 mW								
Average Intensity I:	9.23E+01 kHz/mW								
Peaks	from t	to t	Mean t, s	Mean Rh, nm	mean G, s-1	mean D, cm2s-1	I, kHz/mW	I, % partel <1000nm	
1	1.20E-05	1.20E-05	1.20E-05	1	8.33E+04	2.39E-06	0.05	0%	
2	4.65E-04	6.16E-04	5.60E-04	48	1.79E+03	5.12E-08	9.23	24%	
3	2.51E-03	3.33E-03	2.89E-03	249	3.46E+02	9.91E-09	29.55	76%	
4	3.16E-02	3.16E-02	3.16E-02	2717	3.16E+01	9.07E-10	8.53		
5	1.16E+01	1.16E+01	1.16E+01	>1000	8.62E-02	2.47E-12	44.94		
sum I, partel Rh<1000nm							38.83		
estimated total I, partel Rh<1000nm							776.64		
Isolate #9									
100 000g	dilution:		1:10						
Laser Intensity:	2.05E+00 mW								
Average Intensity I:	1.64E+02 kHz/mW								
Peaks	from t	to t	Mean t, s	Mean Rh, nm	mean G, s-1	mean D, cm2s-1	I, kHz/mW	I, % partel <1000nm	
1	1.40E-05	1.40E-05	1.40E-05	1	7.14E+04	2.05E-06	0.18	0%	
2	6.83E-05	6.83E-05	6.83E-05	6	1.46E+04	4.20E-07	0.25	0%	
3	4.33E-04	7.35E-04	5.90E-04	51	1.70E+03	4.86E-08	17.32	23%	
4	9.57E-04	3.58E-03	2.25E-03	193	4.44E+02	1.27E-08	56.92	76%	
5	6.07E-03	5.82E+00	3.58E+00	>1000	2.79E-01	8.00E-12	89.29		
sum I, partel Rh<1000nm							74.67		
estimated total I, partel Rh<1000nm							746.69		

(Continued)

**Table A2** DLS results of isolates and their corresponding supernatants prepared from frozen/thawed plasma sample; obtained by protocols #6-#10.—cont'd

Isolate #10									
100 000g	dilution:		1:10						
Laser Intensity:	2.06E+00		mW						
Average Intensity I:	1.83E+02		kHz/mW						
Peaks	from t	to t	Mean t, s	Mean Rh, nm	mean G, s-1	mean D, cm2s-1	I, kHz/mW	I, % partcl <1000nm	
1	1.20E-05	1.44E-05	1.27E-05	1	7.90E+04	2.27E-06	0.05	0%	
2	2.08E-05	2.49E-05	2.32E-05	2	4.31E+04	1.23E-06	0.25	1%	
3	1.08E-04	1.55E-04	1.42E-04	12	7.05E+03	2.02E-07	5.32	15%	
4	6.70E-04	9.66E-04	8.29E-04	71	1.21E+03	3.46E-08	30.81	85%	
5	3.47E-03	9.34E-02	4.15E-02	>1000	2.41E+01	6.91E-10	146.19		
sum I, partcl Rh<1000nm							36.42		
estimated total I, partcl Rh<1000nm							364.20		
supernatant #7									
20 000g	dilution:		1:20						
Laser Intensity:	4.60E+00		mW						
Average Intensity I:	6.85E+01		kHz/mW						
Peaks	from t	to t	Mean t, s	Mean Rh, nm	mean G, s-1	mean D, cm2s-1	I, kHz/mW	I, % partcl <1000nm	
1	2.31E-05	3.21E-05	3.05E-05	3	3.28E+04	9.40E-07	2.19	1%	
2	8.61E-05	1.66E-04	1.23E-04	11	8.10E+03	2.32E-07	16.83	7%	
3	4.45E-04	3.19E-03	1.44E-03	123	6.95E+02	1.99E-08	219.74	92%	
4	3.15E+01	3.15E+01	3.15E+01	>1000	3.17E-02	9.10E-13	15.61		
sum I, partcl Rh<1000nm							238.76		
estimated total I, partcl Rh<1000nm							4775.26		
supernatant #8									
50 000g	dilution:		1:20						
Laser Intensity:	1.32E+00		mW						
Average Intensity I:	2.53E+02		kHz/mW						
Peaks	from t	to t	Mean t, s	Mean Rh, nm	mean G, s-1	mean D, cm2s-1	I, kHz/mW	I, % partcl <1000nm	
1	4.45E-05	6.47E-05	4.96E-05	4	2.02E+04	5.78E-07	7.78	3%	
2	1.65E-04	3.49E-04	2.37E-04	20	4.21E+03	1.21E-07	36.67	15%	
3	1.07E-03	2.27E-03	1.50E-03	129	6.65E+02	1.91E-08	198.59	83%	
4	1.16E-01	1.16E-01	1.16E-01	>1000	8.62E+00	2.47E-10	10.39		
sum I, partcl Rh<1000nm							243.03		
estimated total I, partcl Rh<1000nm							4860.68		
supernatant #9									
100 000g	dilution:		1:20						
Laser Intensity:	1.29E+00		mW						
Average Intensity I:	2.55E+02		kHz/mW						
Peaks	from t	to t	Mean t, s	Mean Rh, nm	mean G, s-1	mean D, cm2s-1	I, kHz/mW	I, % partcl <1000nm	
1	1.20E-05	1.20E-05	1.20E-05	1	8.33E+04	2.39E-06	0.12	0%	
2	3.70E-05	4.90E-05	4.26E-05	4	2.35E+04	6.72E-07	3.58	1%	
3	8.59E-05	2.00E-04	1.38E-04	12	7.27E+03	2.08E-07	15.21	6%	
4	2.65E-04	4.41E-03	1.75E-03	151	5.70E+02	1.63E-08	233.61	93%	
sum I, partcl Rh<1000nm							252.51		
estimated total I, partcl Rh<1000nm							5050.16		
supernatant #10									
100 000g	dilution:		1:20						
Laser Intensity:	1.33E+00		mW						
Average Intensity I:	2.61E+02		kHz/mW						
Peaks	from t	to t	Mean t, s	Mean Rh, nm	mean G, s-1	mean D, cm2s-1	I, kHz/mW	I, % partcl <1000nm	
1	2.31E-05	3.21E-05	2.72E-05	2	3.68E+04	1.05E-06	1.34	1%	
2	6.19E-05	1.66E-04	1.01E-04	9	9.95E+03	2.85E-07	15.85	6%	
3	4.44E-04	6.13E-03	1.56E-03	135	6.39E+02	1.83E-08	227.42	93%	
4	1.64E-02	3.17E-02	2.27E-02	1955	4.40E+01	1.26E-09	8.53		
5	8.48E-02	3.12E+01	1.96E+01	>1000	5.10E-02	1.46E-12	7.57		
sum I, partcl Rh<1000nm							244.61		
estimated total I, partcl Rh<1000nm							4892.29		

**Table A3** Association of Alpha-2-macroglobulin (A2M), Apolipoprotein B-100 (APOB), C4b-binding protein alpha chain (C4BPA), Ceruloplasmin (CP), Complement C3 (C3), Complement C4-A (C4.A), Fibronectin (FN1), Immunoglobulin heavy constant gamma 2 (IGHG2), Immunoglobulin heavy constant mu (IGHM), Alpha-1-microglobulin/bikunin precursor (AMBP) and serum albumin (ALB) with membranes, EVs, and microparticles.

Annotation	Protein	Reference	
blood microparticles	CP	PMID:22516433	
	A2M	PMID:22516433	
	C3	PMID:22516433	
	IGHG2	PMID:22516433	
	IGHM	PMID:22516433	
	FN1	PMID:22516433	
	AMBP	PMID:22516433	
	ALB	PMID:22516433	
	C4BPA	PMID:22516433	
	C4A	PMID:22516433	
	C4B	PMID:22516433	
	extracellular exosomes	CP	PMID:23533145. PMID:19056867
		A2M	PMID:23533145. PMID:20458337. PMID:21362503
C3		PMID:23533145. PMID:21362503	
IGHG2		PMID:23533145	
IGHM		PMID:23533145. PMID:19199708	
FN1		PMID:23533145. PMID:21276792. PMID:19056867	
AMBP		PMID:23533145. PMID:19056867	
ALB		PMID:23533145. PMID:21276792. PMID:22516433. PMID:19056867. PMID:20458337. PMID:21362503	
APOB		PMID:23533145	
C4A		PMID:23533145	
C4B		PMID:23533145	
cytoplasmic membrane		CP	PMID:21873635
		C3	Reactome: R-HSA-977615. R-HSA-977371.R-HSA-977371. R-HSA-8853252. R-HSA-8852874. R-HSA-3266557
	IGHG2	GO_REF:0000037. GO_REF: 0000039	
	IGHM	Reactome: R-HSA-983707. R-HSA-983703. R-HSA-983700. R-HSA-983696. R-HSA-9606151.	

(Continued)

**Table A3** Association of Alpha-2-macroglobulin (A2M), Apolipoprotein B-100 (APOB), C4b-binding protein alpha chain (C4BPA), Ceruloplasmin (CP), Complement C3 (C3), Complement C4-A (C4.A), Fibronectin (FN1), Immunoglobulin heavy constant gamma 2 (IGHG2), Immunoglobulin heavy constant mu (IGHM), Alpha-1-microglobulin/bikunin precursor (AMBP) and serum albumin (ALB) with membranes, EVs, and microparticles.—cont'd

Annotation	Protein	Reference
		R-HSA-8858498.
		R-HSA-5690740.
		R-HSA-5690702.
		R-HSA-5690701.
		R-HSA-1112666. GO_REF: 0000037. GO_REF:0000039
	AMBP	PMID:12817471. PMID:21873635
	C4BPA	Reactome: R-HSA-981680. R-HSA-981665. R-HSA-981658. R-HSA-981648. R-HSA-981637. R-HSA-977626
	APOB	Reactome: R-HSA-8871194. R-HSA-8871193. R-HSA- 8869438. R-HSA-8868661. R-HSA-8868660. R-HSA- 8868659. R-HSA-8868658. R-HSA-8868651. R-HSA- 8868648. R-HSA-8868236. R-HSA-8868230. R-HSA- 8868072. R-HSA-8868071. R-HSA-8867756. R-HSA- 8867754. R-HSA-8863471. R-HSA-174706. R-HSA-174657. R-HSA-171141. R-HSA-171122
	C4A	Reactome:R-HSA-981637. R-HSA-977615
	C4B	Reactome:R-HSA-981637. R-HSA-977615
	FN1	GO_REF:0000107
	IGHG2	PMID:21873635
	IGHM	PMID:21873635
positive regulation of	C3	PMID:19302245
apoptotic cell	C4A	PMID:19302245
clearance	C4B	PMID:19302245

## Acknowledgments

Authors acknowledge support from the European Union's Horizon 2020 research and innovation program under grant agreement No. 801338 (VES4US project) and Slovenian Research Agency (ARRS, grants J1-9162, J2-8166, J2-8169, J5-7098, P2-0132, P2-0232, P3-0388, Z2-9215).

## References

- [1] P. Wolf, The nature and significance of platelet products in human plasma, *Br. J. Haematol.* 13 (1967) 269–288.
- [2] M. Yáñez-Mó, P.R.M. Siljander, Z. Andreu, et al., Biological properties of extracellular vesicles and their physiological functions, *J. Extracell. Vesicles* 4 (2015) 27066.
- [3] D. Vozel, B. Uršič, J.L. Krek, R. Štukelj, V. Kralj-Iglič, Applicability of extracellular vesicles in clinical studies, *Eur. J. Clin. Invest.* 47 (2017) 305–313.
- [4] R.E. Lane, D. Korbie, M.M. Hill, M. Trau, Extracellular vesicles as circulating cancer biomarkers: opportunities and challenges, *Clin. Transl. Med.* 7 (2018) 14.
- [5] H. Shao, H. Im, X. Breakefield, R. Weissleder, H. Lee, New Technologies for analysis of extracellular vesicles, *Chem. Rev.* 118 (2018) 1917–1950.
- [6] C. Campanella, C.C. Bavisotto, M. Logozzi, et al., On the choice of the extracellular vesicles for therapeutic purposes, *Int. J. Mol. Sci.* 20 (2019) E236.
- [7] N. Kosaka, A. Kogure, T. Yamamoto, et al., Exploiting the message from cancer: the diagnostic value of extracellular vesicles for clinical applications, *Exp. Mol. Med.* 51 (2019) 31.
- [8] O.P.B. Wiklander, M.Á. Brennan, J. Lötval, X.O. Breakefield, S.E.I. Andaloussi, Advances in therapeutic applications of extracellular vesicles, *Sci. Transl. Med.* 11 (2019) eaav8521.
- [9] E. Serrano-Pertierra, M. Oliveira-Rodríguez, M. Rivas, et al., Characterization of plasma-derived extracellular vesicles isolated by different methods: a comparison study, *Bioengineering* 6 (2019) E8.
- [10] M.Y. Konoshenko, E.A. Lekhnov, A.V. Vlassov, P.P. Laktionov, Isolation of extracellular vesicles: general methodologies and latest trends, *BioMed Res. Int.* 2018 (2018) 8545347.
- [11] T.A. Hartjes, S. Mytnyk, G.W. Jenster, V. van Steijn, M.E. van Royen, Extracellular vesicle quantification and characterization: common methods and emerging approaches, *Bioengineering* 6 (2019) E7.
- [12] D.D. Taylor, S. Shah, Methods of isolating extracellular vesicles impact down-stream analyses of their cargoes, *Methods* 87 (2015) 3–10.
- [13] M.I. Ramirez, M.G. Amorim, C. Gadelha, et al., Technical challenges of working with extracellular vesicles, *Nanoscale* 10 (2018) 881–906.
- [14] K.W. Witwer, E.I. Buzas, L.T. Bemis, et al., Standardization of sample collection, isolation and analysis methods in extracellular vesicle research, *J. Extracell. Vesicles* 2 (2013).
- [15] C. Théry, K.W. Witwer, E. Aikawa, et al., Minimal information for studies of extracellular vesicles 2018 (MISEV2018): a position statement of the International Society for Extracellular Vesicles and update of the MISEV2014 guidelines, *J. Extracell. Vesicles* 7 (2018) 1535750.
- [16] M. Venturella, F.M. Carpi, D. Zocco, Standardization of blood collection and processing for the diagnostic use of extracellular vesicles, *Curr. Pathobiol. Rep.* 7 (2019) 1–8.
- [17] V. Šuštar, A. Bedina-Zavec, R. Štukelj, et al., Nanoparticles isolated from blood: a reflection of vesiculability of blood cells during the isolation process, *Int. J. Nanomed.* 6 (2011) 2737–2748.

- [18] M. Monguió-Tortajada, C. Gálvez-Montón, A. Bayes-Genis, S. Roura, F.E. Borràs, Extracellular vesicle isolation methods: rising impact of size-exclusion chromatography, *Cell. Mol. Life Sci.* 76 (2019) 2369–2382.
- [19] T. Baranyai, K. Herczeg, Z. Onódi, et al., Isolation of exosomes from blood plasma: qualitative and quantitative comparison of ultracentrifugation and size exclusion chromatography methods, *PLoS One* 10 (2015) e0145686.
- [20] L. Musante, M. Saraswat, A. Ravidà, B. Byrne, H. Holthofer, Recovery of urinary nanovesicles from ultracentrifugation supernatants, *Nephrol. Dial. Transplant.* 28 (2012) 1425–1433.
- [21] Z. Onódi, et al., Isolation of high-purity extracellular vesicles by the combination of iodixanol density gradient ultracentrifugation and bind-elute chromatography from blood plasma, *Front. Physiol.* 9 (2018) 1479.
- [22] N. Karimi, A. Cvjetkovic, S.C. Jang, R. Crescitelli, M.A. Hosseinpour Feizi, R. Nieuwland, J. Lötvall, C. Lässer, Detailed analysis of the plasma extracellular vesicle proteome after separation from lipoproteins, *Cell. Mol. Life Sci.* 75 (2018) 2873–2886.
- [23] A. Abramowicz, P. Widlak, M. Pietrowska, Proteomic analysis of exosomal cargo: the challenge of high purity vesicle isolation, *Mol. Biosyst.* 12 (2016) 1407–1419.
- [24] J. Van Deun, P. Mestdagh, R. Sormunen, et al., The impact of disparate isolation methods for extracellular vesicles on downstream RNA profiling, *J. Extracell. Vesicles* 3 (2014) 24858.
- [25] R. Linares, S. Tan, C. Gounou, N. Arraud, A.R. Brisson, High-speed centrifugation induces aggregation of extracellular vesicles, *J. Extracell. Vesicles* 4 (2015) 29509.
- [26] J.Z. Nordin, Y. Lee, P. Vader, et al., Ultrafiltration with size-exclusion liquid chromatography for high yield isolation of extracellular vesicles preserving intact biophysical and functional properties, *Nanomedicine* 11 (2015) 879–883.
- [27] S.I. Brett, F. Lucien, C. Guo, et al., Immunoaffinity based methods are superior to kits for purification of prostate derived extracellular vesicles from plasma samples, *Prostate* 77 (2017) 1335–1343.
- [28] P. Sharma, S. Ludwig, L. Muller, et al., Immunoaffinity-based isolation of melanoma cell-derived exosomes from plasma of patients with melanoma, *J. Extracell. Vesicles* 7 (2018) 1435138.
- [29] A. Clayton, J. Court, H. Navabi, et al., Analysis of antigen presenting cell derived exosomes, based on immuno-magnetic isolation and flow cytometry, *J. Immunol. Methods* 247 (2001) 163–174.
- [30] Y. Tian, M. Gong, Y. Hu, et al., Quality and efficiency assessment of six extracellular vesicle isolation methods by nano-flow cytometry, *J. Extracell. Vesicles* 9 (2020) 1697028.
- [31] D. Freitas, M. Balmaña, J. Poças, et al., Different isolation approaches lead to diverse glycosylated extracellular vesicle populations, *J. Extracell. Vesicles* 8 (2019) 1621131.
- [32] R.J. Berckmans, R. Nieuwland, A.N. Boeing, et al., Cell-derived microparticles circulate in healthy humans and support low grade thrombin generation, *Thromb. Haemostasis* 85 (2001) 639–646.
- [33] M. Diamant, R. Nieuwland, R.F. Pablo, et al., Elevated numbers of tissue-factor exposing microparticles correlate with components of the metabolic syndrome in uncomplicated type 2 diabetes mellitus, *Circulation* 106 (2002) 2442–2447.
- [34] C.A.R. Lok, A.N. Böing, P.H. Reitsma, et al., Expression of inflammation-related genes in endothelial cells is not directly affected by microparticles from preeclamptic patients, *J. Lab. Clin. Med.* 147 (2006) 310–320.
- [35] B. Toth, K. Nikolajek, A. Rank, et al., Gender-specific and menstrual cycle dependent differences in circulating microparticles, *Platelets* 18 (2007) 515–521.

- [36] R.J. Berckmans, R. Nieuwland, P.P. Tak, et al., Cell-derived microparticles in synovial fluid from inflamed arthritic joints support coagulation exclusively via a factor VII-dependent mechanism, *Arthritis Rheum.* 46 (2002) 2857–2866.
- [37] R.J. Berckmans, R. Nieuwland, M.C. Kraan, et al., Synovial microparticles from arthritic patients modulate chemokine and cytokine release by synoviocytes, *Arthritis Res. Ther.* 7 (2005) R536–R544.
- [38] R.J. Berckmans, A. Sturk, L.M. Van Tienen, M.C. Schaap, R. Nieuwland, Cell-derived vesicles exposing coagulant tissue factor in saliva, *Blood* 117 (2011) 3172–3180.
- [39] I. Junkar, V. Utar, M. Frank-Bertoncelj, et al., Blood and synovial microparticles as revealed by atomic force and scanning electron microscope, *Open Autoimmun. J.* 1 (2009) 50–58.
- [40] É. Biró, K.N. Sturk-Maquelin, G.M.T. Vogel, et al., Human cell-derived microparticles promote thrombus formation in vivo in a tissue factor-dependent manner, *J. Thromb. Haemostasis* 1 (2003) 2561–2568.
- [41] E.A.J. Knijff-Dutmer, J. Koerts, R. Nieuwland, E.M. Kalsbeek-Batenburg, M.A.F.J. Van De Laar, Elevated levels of platelet microparticles are associated with disease activity in rheumatoid arthritis, *Arthritis Rheum.* 46 (2002) 1498–1503.
- [42] K. Schara, R. Štukelj, J.L. Krek, et al., A study of extracellular vesicle concentration in active diabetic Charcot neuroarthropathy, *Eur. J. Pharm. Sci.* 98 (2017) 58–63.
- [43] R. Štukelj, K. Schara, A. Bedina – Zavec, et al., Effect of shear stress in the flow through the sampling needle on concentration of nanovesicles isolated from blood, *Eur. J. Pharm. Sci.* 98 (2017) 17–29.
- [44] A. Mrvar-Brečko, V. Šuštar, V. Janša, et al., Isolated microparticles from peripheral blood and body fluids as observed by scanning electron microscope, *Blood Cells Mol. Dis.* 44 (2010) 307–312.
- [45] S. Liebhardt, N. Ditsch, R. Nieuwland, et al., CEA-, Her2/neu-, BCRP- and Hsp27-positive microparticles in breast cancer patients, *Anticancer Res.* 30 (2010) 1707–1712.
- [46] B. Toth, R. Nieuwland, S. Liebhardt, et al., Circulating microparticles in breast cancer patients: a comparative analysis with established biomarkers, *Anticancer Res.* 28 (2008) 1107–1112.
- [47] V. Lešer, D. Drobne, Ž. Pipan, M. Milani, F. Tatti, Comparison of different preparation methods of biological samples for FIB milling and SEM investigation, *J. Microsc.* 233 (2009) 309–319.
- [48] S. Sitar, V. Aseyev, K. Kogej, Differences in association behavior of isotactic and atactic poly(methacrylic acid), *Polymer* 55 (2014) 848–854.
- [49] S. Sitar, V. Aseyev, K. Kogej, Microgel-like aggregates of isotactic and atactic poly(methacrylic acid) chains in aqueous alkali chloride solutions as evidenced by light scattering, *Soft Matter* 10 (2014) 7712–7722.
- [50] D. Božič, S. Sitar, I. Junkar, et al., Viscosity of plasma as a key factor in assessment of extracellular vesicles by light scattering, *Cells* 8 (2019) E1046.
- [51] S.W. Provencher, CONTIN: a general purpose constrained regularization program for inverting noisy linear algebraic and integral equations, *Comput. Phys. Commun.* 27 (1982) 229–242.
- [52] G. Pocsfalvi, L. Turiák, A. Ambrosone, et al., Protein biocargo of citrus fruit juice sac cells-derived vesicles reveals heterogeneous transport and extracellular vesicle subpopulations, *J. Plant Physiol.* 229 (2018) 111–121.
- [53] C. Stanly, M. Moubarak, I. Fiume, L. Turiák, G. Pocsfalvi, Membrane transporters in citrus clementina fruit juice-derived nanovesicles, *Int. J. Mol. Sci.* 20 (2019) E6205.
- [54] G. Pocsfalvi, C. Stanly, A. Vilasi, et al., Mass spectrometry of extracellular vesicles, *Mass Spectrom. Rev.* 35 (2016) 3–21.

- [55] V. Kralj-Iglic, Stability of membranous nanostructures: a possible key mechanism in cancer progression, *Int. J. Nanomed.* 7 (2012) 3579–3596.
- [56] S. Principe, E.E. Jones, Y. Kim, et al., In-depth proteomic analyses of exosomes isolated from expressed prostatic secretions in urine, *Proteomics* 13 (2013) 1667–1671.
- [57] S.I. Buschow, B.W. van Balkom, M. Aalberts, et al., MHC class II-associated proteins in B-cell exosomes and potential functional implications for exosome biogenesis, *Immunol. Cell Biol.* 88 (2010) 851–856.
- [58] W.D. Stamer, E.A. Hoffman, J.M. Luther, D.L. Hachey, K.L. Schey, Protein profile of exosomes from trabecular meshwork cells, *J. Proteom.* 74 (2011) 796–804.
- [59] P. Bastos-Amador, F. Royo, E. Gonzalez, et al., Proteomic analysis of microvesicles from plasma of healthy donors reveals high individual variability, *J. Proteomics* 75 (2012) 3574–3584.
- [60] P.A. Gonzales, T. Pisitkun, J.D. Hoffert, et al., Large-scale proteomics and phospho-proteomics of urinary exosomes, *J. Am. Soc. Nephrol.* 20 (2009) 363–379.
- [61] S. Atay, C. Gercel-Taylor, M. Kesimer, D.D. Taylor, Morphologic and proteomic characterization of exosomes released by cultured extravillous trophoblast cells, *Exp. Cell Res.* 317 (2011) 1192–1202.
- [62] M.P. Caby, D. Lankar, C. Vincendeau-Scherrer, G. Raposo, C. Bonnerot, Exosomal-like vesicles are present in human blood plasma, *Int. Immunol.* 17 (2005) 879–887.
- [63] S. Strohkamp, T. Gemoll, J.K. Habermann, Possibilities and limitations of 2DE-based analyses for identifying low-abundant tumor markers in human serum and plasma, *Proteomics* 16 (2016) 2519–2532.
- [64] D. Binns, E. Dimmer, R. Huntley, et al., QuickGO: a web-based tool for Gene Ontology searching, *Bioinformatics* 25 (2009) 3045–3046.
- [65] E. Boilard, A.C. Duchez, A. Brisson, The diversity of platelet microparticles, *Curr. Opin. Hematol.* 22 (2015) 437–444.
- [66] N. Arraud, R. Linares, S. Tan, et al., Extracellular vesicles from blood plasma: determination of their morphology, size, phenotype and concentration, *J. Thromb. Haemostasis* 12 (2014) 614–627.
- [67] M.T. Aatonen, T. Öhman, T.A. Nyman, et al., Isolation and characterization of platelet-derived extracellular vesicles, *J. Extracell. Vesicles* 3 (2014) 24692.
- [68] H.F. Heijnen, A.E. Schiel, R. Fijnheer, H.J. Geuze, J.J. Sixma, Activated platelets release two types of membrane vesicles: microvesicles by surface shedding and exosomes derived from exocytosis of multivesicular bodies and alpha-granules, *Blood* 94 (1999) 3791–3799.
- [69] K. Joop, R.J. Berckmans, R. Nieuwland, et al., Microparticles from patients with multiple organ dysfunction syndrome and sepsis support coagulation through multiple mechanisms, *Thromb. Haemostasis* 85 (2001) 810–820.
- [70] I. Melki, N. Tessandier, A. Zufferey, E. Boilard, Platelet microvesicles in health and disease, *Platelets* 28 (2017) 214–221.
- [71] P.S. Sung, T.F. Huang, S.L. Hsieh, Extracellular vesicles from CLEC2-activated platelets enhance dengue virus-induced lethality via CLEC5A/TLR2, *Nat. Commun.* 10 (2019) 2402.
- [72] B. Fendl, R. Weiss, M.B. Fischer, A. Spittler, V. Weber, Characterization of extracellular vesicles in whole blood: influence of pre-analytical parameters and visualization of vesicle-cell interactions using imaging flow cytometry, *Biochem. Biophys. Res. Commun.* 478 (2016) 168–173.
- [73] A.P. Bode, C.L. Knupp, Effect of cold storage on platelet glycoprotein Ib and vesiculation, *Transfusion* 34 (1994) 690–696.
- [74] J. Steinkühler, E. Sezgin, I. Urbančić, C. Eggeling, R. Dimova, Mechanical properties of plasma membrane vesicles correlate with lipid order, viscosity and cell density, *Commun. Biol.* 2 (2019) 337.

- [75] S.L. Veatch, P. Cicuta, P. Sengupta, et al., Critical fluctuations in plasma membrane vesicles, *ACS Chem. Biol.* 3 (2008) 287–293.
- [76] R. Zarka, M.B. Horev, T. Volberg, et al., Differential modulation of platelet adhesion and spreading by adhesive ligand density, *Nano Lett.* 19 (2019) 1418–1427.
- [77] V. Leytin, Apoptosis in the anucleate platelet, *Blood Rev.* 26 (2012) 51–63.
- [78] R. Nieuwland, R.J. Berckmans, R.C. Rotteveel-Eijkman, et al., Cell-derived microparticles generated in patients during cardiopulmonary bypass are highly procoagulant, *Circulation* 96 (1997) 3534–3541.
- [79] A.J. Reininger, H.F. Heijnen, H. Schumann, et al., Mechanism of platelet adhesion to von Willebrand factor and microparticle formation under high shear stress, *Blood* 107 (2006) 3537.
- [80] Y. Miyazaki, S. Nomura, T. Miyake, et al., High shear stress can initiate both platelet aggregation and shedding of procoagulant containing microparticles, *Blood* 88 (1996) 3456–3464.
- [81] A. Pal, D.V. Khakhar, Breakage of vesicles in a simple shear flow, *Soft Matter* 15 (2019) 1979–1987.
- [82] T. Nielsen, A.F. Kristensen, S. Pedersen, G. Christiansen, S.R. Kristensen, Investigation of procoagulant activity in extracellular vesicles isolated by differential ultracentrifugation, *J. Extracell. Vesicles* 7 (2018) 1454777.
- [83] R.W. Stroetz, N.E. Vlahakis, B.J. Walters, M.A. Schroeder, R.D. Hubmayr, Validation of a new live cell strain system: characterization of plasma membrane stress failure, *J. Appl. Physiol.* 90 (2001) 2361–2370.
- [84] O.E. Olorundare, O. Peyruchaud, R.M. Albrecht, D.F. Mosher, Assembly of a fibronectin matrix by adherent platelets stimulated by lysophosphatidic acid and other agonists, *Blood* 98 (2001) 117–124.
- [85] W.S. To, K.S. Midwood, Plasma and cellular fibronectin: distinct and independent functions during tissue repair, *Fibrogenesis Tissue Rep.* 4 (2011) 21.
- [86] T.T. Nguyen Huong, C. Huynh Khon, E. Scharf Rüdiger, R. Stoldt Volker, *Biol. Chem.* 394 (2013) 1495.
- [87] H. Nguyen, K. Huynh, V.R. Stoldt, Shear-dependent fibrillogenesis of fibronectin: impact of platelet integrins and actin cytoskeleton, *Biochem. Biophys. Res. Commun.* 497 (2018) 797–803.
- [88] E.I. Buzás, E.Á. Tóth, B.W. Sódar, K.É. Szabó–Taylor, Molecular interactions at the surface of extracellular vesicles, *Semin. Immunopathol.* 40 (2018) 453–464.
- [89] G. Kushwaha, S.N. Chaurasia, A. Pandey, D. Dash, Characterization of fibrinogen binding on platelet-derived extracellular vesicles, *Thromb. Res.* 172 (2018) 135–138.
- [90] S.P. Jackson, The growing complexity of platelet aggregation, *Blood* 109 (2007) 5087.
- [91] I. Furi, F. Momen-Heravi, G. Szabo, Extracellular vesicle isolation: present and future, *Ann. Transl. Med.* 5 (2017), 263–263.
- [92] E. Biró, R. Nieuwland, P.P. Tak, et al., Activated complement compounds and complement activator molecules on the surface of cell-derived microparticles in patients with rheumatoid arthritis and healthy individuals, *Ann. Rheum. Dis.* 66 (2007) 1085–1092.
- [93] M.J. Justice, D.N. Petrusca, A.L. Rogozea, et al., Effects of lipid interactions on model vesicle engulfment by alveolar macrophages, *Biophys. J.* 106 (2014) 598–609.
- [94] D. Božič, M. Hočevar, V. Kononenko, M. Jeran, U. Stibler, I. Fiume, M. Pajnič, L. Pađen, K. Kogej, D. Drobne, A. Igljč, G. Pocsfalvi, V. Kralj-Igljč, Effect of ultracentrifuge systemic force on extracellular vesicle isolates from blood plasma, (in preparation).